CHAPTER II

NASA-LMT HISTORY

The NASA-LMT was conceived in 1990 as a low-cost, large aperture telescope that would be dedicated to observing orbital objects. Using this telescope, NASA could better fulfill its mission to promote space exploration via a more thorough characterization of the orbital environment and thereby provide a more accurate assessment of the potential hazard to spacecraft from collisions and the protection needed. The telescope's role has since evolved to include comprehensive observations of astronomical objects as well as a planned survey of Near Earth Objects (NEOs). The development of the NASA-LMT, from the initial proposal within the framework of the orbital debris problem, to early proof of concept at NASA-JSC, through fully operational status at NODO, is described herein.

A. Orbital Space Debris

To place the NASA-LMT in context, a brief treatment of orbital debris detection and research is provided. Orbital space debris has been accumulating since the launch of Sputnik in 1957 and consists of all orbiting objects other than operational satellites. Distributed at various altitudes and orbital inclinations, it is composed of a wide array of both intact and disrupted objects of various shapes and sizes and materials. Examples include inactive payloads, spent rocket bodies, and explosion byproducts such as wiring

harnesses, fasteners, disrupted fuel tanks, and shrouds. These objects, as well as the micrometeoroid background, present a hazard to human space flight activities and therefore are of interest to NASA in its mission to promote space exploration.

The specific hazard to spacecraft arises from the risk of high-speed collisions. The damage resulting from even a small object colliding with a spacecraft can be catastrophic due to the high relative velocity of impact. A 1.0 cm diameter solid aluminum sphere (of mass 1.41 grams (g)) traveling at a typical low earth orbit (LEO) velocity of 7.0 kilometers per second (km/s) has the same kinetic energy as a 1000 kilogram (kg) object (eg. a car) traveling at 30 kilometers per hour (km/hr). Even a fleck of paint can cause damage as indicated by the numerous Space Shuttle windshields that have been replaced due to craters formed by collisions with orbiting paint chips or micrometeoroids (Kessler 1993). To illustrate the potential threat to spacecraft or a spacesuit, Figure II.A-1 shows a 2.5 cm thick aluminum (Al) plate that was struck with a 1.5 g Al disk travelling at 1.5 km/s.

Studying the population of orbiting objects began during the cold war. After the launch of Sputnik, the United States (US) developed a global network of RADAR installations and optical observatories whose mission was to catalogue and track the rapidly growing orbital population of satellites, spent rocket bodies, and debris pieces generated from payload ejections, rocket body explosions, and collisions. Initially, the observations enabled the US to stay apprised of progress made by the Union of Soviet Socialist Republics (USSR) and provided a rudimentary early warning system for incoming Intercontinental Ballistic Missiles (ICBMs). As time has progressed the

NASA-JSC Hypervelocity Impact Test Facility (HITF) Sample

Figure II.A-1. The impact crater on a stationary 2.5 cm thick aluminum plate resulting from a collision with a 1.5 gram, 1.6 cm diameter aluminum disk, traveling at 1.5 km/sec. The kinetic energy of the disk was 1688 Joules, significantly less than the 50,000 Joule kinetic energy typical of an identical particle involved in an orbital collision.

network has monitored the threat of anti-satellite activities, spy-satellites, and the increasing hazard posed by orbital debris to space-faring activities. This US Space Surveillance Network (SSN) has grown to include stations distributed globally with sites in Diego Garcia, Kwajelein Island, Maui, New Mexico, Florida, and North Dakota. It is operated by Air Force Space Command from the North American Aerospace Defense Command (NORAD) center located at Cheyenne Mountain in Colorado Springs, Colorado.

The SSN was originally designed to track and catalogue only those objects perceived as a strategic threat and thus the instruments and their sensitivity were optimized to detect objects with sizes 10 cm diameter or greater. Furthermore, the altitude range was delimited into three zones of interest: low-earth orbit (LEO; <2000 km), middle-earth orbit (MEO; 2000 km-20,000 km), and Geo-synchronous orbit (GEO; 22,500 km), with primary interest in the LEO region. To this end, the backbone of the SSN still consists today of UHF (440MHz) 68 centimeter (cm) wavelength RADAR which are optimal for detecting LEO objects with small dielectric constants (eg. metallic) and sizes comparable to the wavelength employed - placing them above the Rayleigh scattering regime into the region of Mie (Kerker 1969; Van de Hulst 1981) or optical scattering. Figures II.A-2 and 3 illustrate the limitations of low-frequency RADAR and the advantages of higher-frequency operation in the detection of small objects.

In effort to detect a wider range of object materials and at higher altitudes, the SSN also includes optical telescopes. Since the RADAR is an active detector, they have poor sensitivity at high altitudes because the beam power from the antenna and the

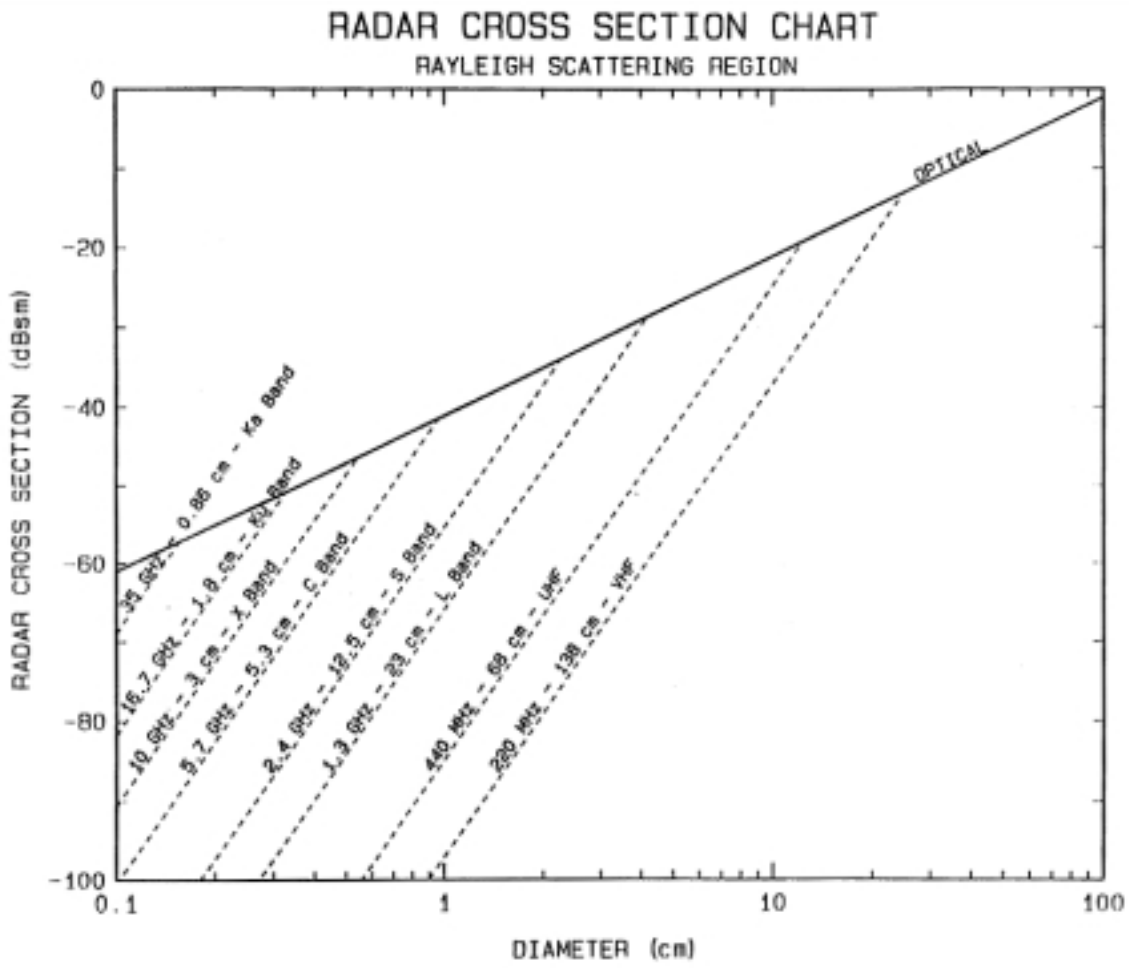

Figure II.A-2. A plot illustrating RADAR Cross-Section (Decibels/m^2) as a function of physical object diameter for a variety of RADAR employed in the tracking and cataloguing of orbiting objects. The UHF RADAR, which comprises the backbone of the SSN, rapidly loses sensitivity for object diameters below 10 cm. Higher frequency RADAR are required to sample the smaller orbital population. Chart courtesy NASA.

RADAR Cross-section (RCS) Measurements of Representative Orbital Debris Objects

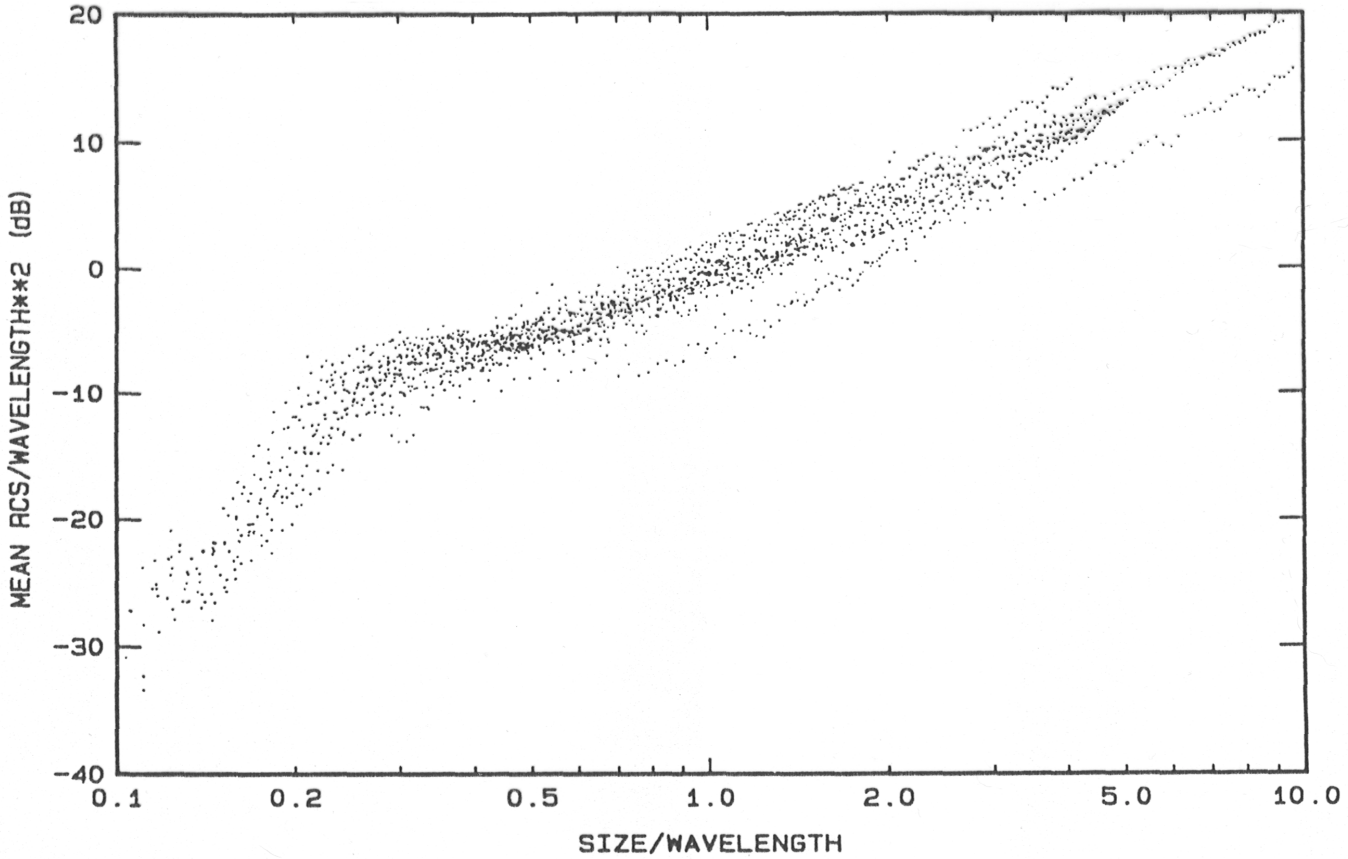

Figure II.A-3. A plot illustrating the empirical results of RADAR Cross-Section measurements as a function of physical object diameter for a variety of RADAR employed in the tracking and cataloguing of orbiting objects. The plot is normalized to show the intrinsic sensitivity loss when object size falls into the Rayleigh regime below approximately 30% of the RADAR operating wavelength. This plot was generated using a suite of RADAR (λ =1.67 – 15 cm) and 39 representative debris fragments of varying size. Each point represents a single object measured at a single frequency. Chart courtesy NASA.

reflected power from the object both fall off as the square of the distance ($1/r^2$) yielding a forth-power dependency of sensitivity on inverse distance ($1/r^4$). Passive optical telescopes, which rely on sunlight to illuminate debris and thus have only an inverse distance squared dependence on sensitivity ($1/r^2$), were needed to monitor MEO and GEO. Their detection sensitivity is also dependent upon optical reflectivity (albedo) and independent of dielectric constant or material type, giving them a broader material detection ability.

To facilitate the expanded altitude and material sampling, the RADAR are thus complimented by a series of 1.0 meter diameter optical telescopes which comprise the Ground-based Electro-optical Deep Space Surveillance (GEODSS) network. Normally configured with photo-multiplier image tubes (Westinghouse Ebsicons) these telescopes reach a 16.0 magnitude detection limit, corresponding to a 3.6 cm diameter debris object with an albedo of 0.1 at 1000 km altitude or a 72 cm diameter object at 20,000 km. To improve performance the photo-multipliers are gradually being upgraded with more sensitive high-speed CCDs (Africano PC). Since the performance of the GEODSS telescopes is the standard by which all other optical telescopes engaged in orbital debris research are compared, the NASA-LMT had to meet or exceed GEODSS detection capabilities to remain a viable concept.

Although they can operate at all altitude ranges, GEODSS telescopes are primarily employed for MEO and GEO monitoring. They are limited for LEO observing because the earth's shadow eclipses LEO objects progressively after nightfall with increasing solar depression angle (and conversely as dawn approaches). For this reason,

LEO observations with all optical telescopes are limited to conditions near astronomical twilight where the solar depression angle varies from 12 to 18 degrees and the earth's shadow height varies from approximately 100 to 500 km. The active RADAR has a significant advantage in this regard, since it can continuously monitor all LEO altitudes both day and night.

As conceived, the Ku-Band radar and GEODSS telescopes together provide good coverage of only the large orbital object environment. Using the two in conjunction, US Space Command maintains a continually updated satellite catalogue (SATCAT) of orbital debris objects down to an approximate limiting diameter of 10 cm. This catalogue is a primary input to the assessment of the risk that orbital objects pose to orbiting spacecraft. For example, it is the basis for all Space Shuttle collision avoidance maneuvers. The SATCAT is not complete however because the network does not perform uniformly for all object sizes, altitudes or material compositions. The Ku-Band radar, which provides the dominant input to the database, detects high radar cross-section (RCS) LEO objects with confidence (eg. large metallic objects, wires, etc.), but sensitivity diminishes rapidly as object size falls below 10 cm diameter or for objects of high dielectric composition. The GEODSS network concentrates on GEO and MEO where it detects small objects with high optical cross-section (OCS), but misses targets such as some LEO objects, small metallic objects (eg. bolts, wires), or soot-covered explosion byproducts (small albedo) of any material. The incompleteness of the SATCAT is well documented. Henize and Stanley (1990) compared events from 81 hours of blind staring data from GEODSS optical telescopes with the catalogue predictions and found that at object

diameters below 30 cm, the catalogue is less than 25% complete, and no more than 66% complete for object diameters between 30 and 100 cm. Other telescopes, including the NASA-LMT (Africano et al. 1999), have obtained similar results (Chapter VI).

The SATCAT incompleteness can be constrained to three primary causes. First, the radar and optical telescopes by their nature detect different elements of the population. Many orbital objects have sufficient optical cross-section (OCS) and radar cross-section (RCS) to be detectable by both instruments, but there are populations of objects whose detection is unique to only one type of instrument or invisible to both. Second, the optimal operating ranges for the radar and optical telescopes are different so they don't sample the same altitudes. Third, the Ku-Band, RADAR has poor detection sensitivity at smaller sizes. Because of these limitations, the SATCAT must be supplemented with additional data from a variety of other RADAR and optical telescopes to generate a more complete picture of the orbital debris environment. These issues first received significant attention by Don Kessler at NASA-Johnson Space Center in 1963 (Kessler 1993a). Since that time concern has intensified in concert with the expanding awareness about the risk posed to spacecraft and human space flight by orbital debris.

With the advent of the Space Shuttle program and Space Station Freedom (SSF), NASA took the initiative in better characterizing the orbital debris environment. The ability to observe smaller pieces of debris than those in the SATCAT prompted construction of the Haystack Long-Range Imaging RADAR (LRIR) in Millstone, Massachusetts. This Ka Band RADAR operating at 16.7 GHz with a 1.8 cm wavelength has routinely observed debris objects as small as 1 mm diameter since 1995 and has

helped compensate for the most severe SATCAT limitation - size restriction. It is NASA's primary source of information on the size and altitude distribution for the LEO population of small debris (Stansbery et al. 1991).

Characterizing the optical population at various altitudes requires optical telescopes besides GEODSS. The transportable NASA-CCD Debris Telescope (NASA-CDT), a 32 cm diameter Schmidt camera (Figure II.A-4), was developed by Henize primarily to study the optical properties of objects already contained in the SATCAT. The published RADAR cross-sections were used as fiduciary physical cross-sections in order to determine object optical albedos and phase functions for objects with RCS derived sizes as small as 10 cm diameter (Henize et al.1994; Mulrooney 1993). The efforts of Henize contributed significantly to the generally accepted mean optical albedo value for orbital debris of 0.10 ± 0.02.

The NASA-CDT is now operated at NODO where it routinely observes orbital objects at GEO as small as 20 cm (OCS derived) diameter in an effort to characterize the hazard to Geo-stationary satellites posed by non-operational payloads, rocket bodies and disrupted objects. Its work in this regard is a direct compliment to that of GEODSS. Prior to moving to NODO, the CDT was co-located for three years with the GEODSS telescopes at the Air Force Space Surveillance site on Maui, Hawaii. The CDT participated in 5 multi-week observing campaigns wherein dozens of detections were made of uncorrelated targets (UCTs) which were subsequently directed to GEODSS for tracking and ultimate insertion as new objects in the SATCAT.

Numerous other instruments have contributed to the understanding of the orbital

NASA-CDT: 32 cm Schmidt Camera w/ Tri-axial Mount

Figure II.A-4. Photograph of the NASA-CCD Debris Telescope (NASA-CDT). This 32 cm diameter Schmidt camera has a three-axis mounting developed by Jim Wray enabling it to track orbiting objects . It is presently installed at NODO where it primarily searches for orbital debris at GEO altitudes.

object environment. Space borne platforms like the Long Duration Exposure Facility (LDEF) (Kessler 1993b) or the Space Shuttle give in situ information about the orbital debris environment and the risk of collision. Proposed instruments like the space-based telescopic Debris Collision Warning Sensor (DCWS) (Vilas and Talent PC) offer new possibilities.

In the mean time the NASA-LMT occupies a unique niche among those instruments observing orbital objects in terms of both its capabilities and its design. It is the largest optical telescope dedicated to observing orbital debris and in that capacity has detected smaller orbiting objects than any other dedicated optical instrument.

B. NASA-LMT – JSC Development

The NASA-LMT began inauspiciously in 1989, when NASA-Johnson Space Center (JSC) sub-contractor David Talent attended a conference at which Ermanno Borra presented some of his LMT results (Talent PC). Talent reported his impressions to NASA-JSC Branch Chief Drew Potter who was intrigued at the possibility of building an inexpensive, wide-field, large-aperture optical telescope to perform observations of orbital debris. To further explore the prospects, Potter and Lockheed Engineering Sciences Corporation (LESC) engineer Terry Byers arranged a visit to Laval Universite to tour Borra's laboratory. Borra described in detail the construction and operation of the 1.5 meter liquid mirror test bed in place at that time and showed numerous interferograms quantifying the excellent image quality exhibited by the laboratory liquid mirror. Potter

and Byers returned to NASA-JSC convinced of the viability of the LMT concept and Potter allocated $100K to fund early development work to be performed by LESC on what was initially called the Liquid Metal Mirror Telescope (LMMT) project and later simply the NASA-LMT.

From the outset it was desirable that the new orbital debris telescope be able to detect objects smaller than the ostensible 10 cm diameter size limit of the SATCAT. For a minimum detection limit, a 1 cm diameter size was selected because research performed at NASA-JSC on shielding for the SSF indicated that layered bumpers could protect the spacecraft from objects smaller than this. Known as Whipple bumpers, these shields consist of alternating air spaces and sheets of tough but lightweight material (eg. Carbon fiber or Kevlar). Orbital objects impinging on the shield are disrupted by the successive layers turning them into a broad spray of particles which exerts much lower force per unit area when finally striking the spacecraft hull and thus there is much less likelihood of penetration. Since the SSF would be constructed in LEO at approximately 500 km altitude, the planned NASA-LMT would focus on providing information on the LEO debris population in the critical 1 cm to 10 cm diameter size niche - above the 1 cm diameter shielding limit and below the 10 cm diameter SATCAT limit. The LMT would also help to quantify the statistical accuracy of the SATCAT by comparing the observed and predicted flux of objects larger than 10 cm diameter at LEO and MEO altitudes.

Meeting these criterion required that certain conditions be met regarding primary mirror size, focal length, detector quantum efficiency, band width, plate-scale, and total system throughput. Detection sensitivity calculations (Appendix A) indicated that if

located at a dark location with minimal sky brightness, a 78% reflective mercury telescope with a 3.0m diameter primary mirror, a 3 element corrector, and a 4.5 m focal length (f/1.5), coupled to a 2048x2048 (2K) 15um pixel CCD with 35% V Band quantum efficiency (QE) could detect, at a signal-to-noise ration (SNR) of 6.3, a solar illuminated 0.9 cm diameter specular sphere with 0.1 albedo at an altitude of 800 km. This performance at LEO was only possible with a drift-scanning, or TDI mode, CCD set to read at a rate and direction which exactly matched the angular velocity and position angle (PA) of motion of the orbiting object (hereafter Drift Matching or DM mode). Only in this way could all the signal photons accumulate on a few pixels to maximize the signal-to-noise ratio (SNR), rather than streak across the detector as is normal for a fixed telescope and a framing or sidereal scanning CCD. For orbital debris objects moving at rates or PAs other than that selected for DM, the detection efficiency is also poor.

Figures II.B-1 through II.B-6 illustrate the initial white-light idealized performance predictions for the LMT with the CCD in DM , Sidereal rate drift-scanning, and Single Framing mode. Various detection limits are expressed in terms of limiting object size and apparent magnitude for objects traveling at arbitrary rates and directions to a selected CCD read rate and direction (DM or sidereal) or to a framing CCD with exposure times of 3 and 300 seconds. Different sky brightness values corresponding to different observatory locations are also considered. From these graphs it is evident that maximum sensitivity is obtained when exact DM occurs: sensitivity is dramatically enhanced for orbiting objects co-moving with the electro-optically tracking CCD while sensitivity is diminished for other objects. (Appendix B lists the FORTRAN77 program

NASA-LMT @ JSC: Limiting Detection Magnitude versus
Range and Inclination - DM Height = 800 km

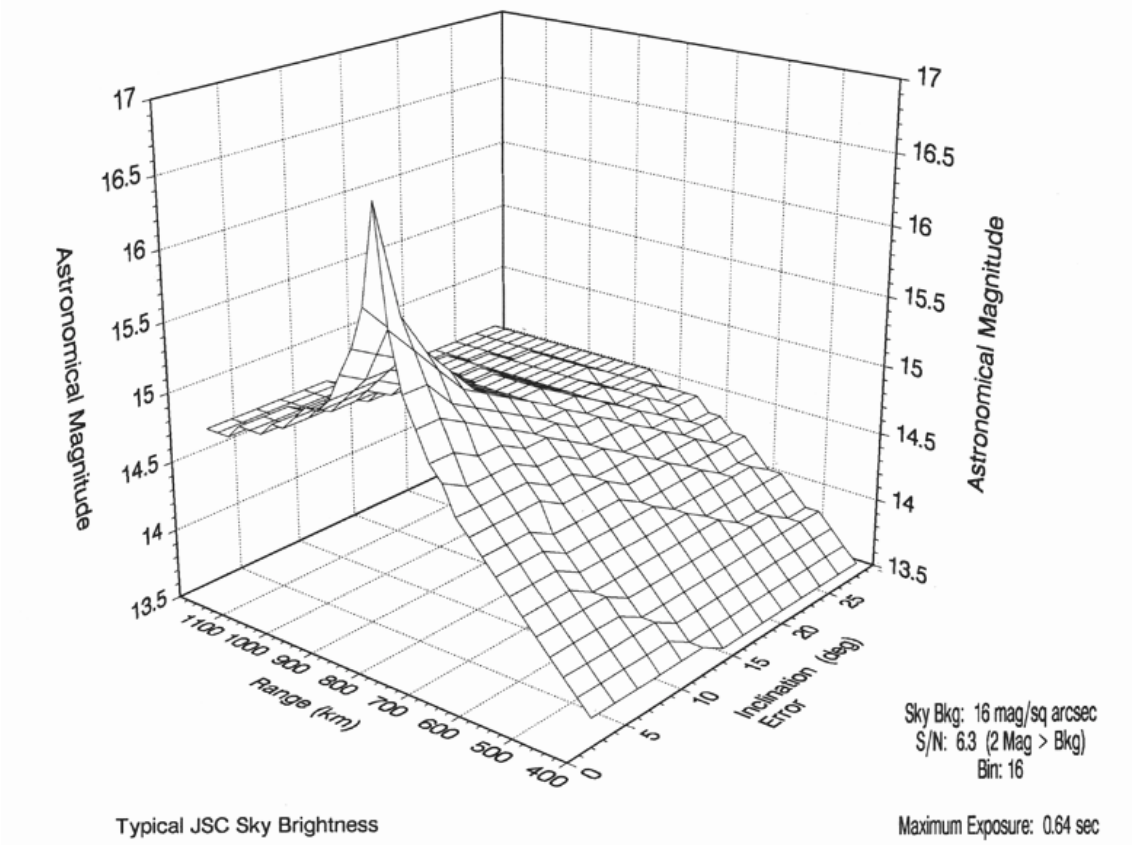

Figure II.B-1. Graph illustrating the advantage of using a CCD in Drift Matching (DM) mode to detect orbital objects. An object passing through the telescope FOV at an angular rate equal to the TDI scan rate and at the same Position Angle (PA) of motion as the CCD read direction, will have its signal photons concentrated on a few pixels rather than spread along the entire FOV. The signal-to-noise ratio (SNR) is maximized and fainter objects can be detected. The sharp peak in apparent magnitude is for an object at the DM rate and direction. Sensitivity, rapidly diminishes for objects moving in other directions and rates. This plot was generated using the typically high (16.0 mag/sq. arcsec) JSC sky brightness.

NASA-LMT @ JSC: Limiting Detection Diameter versus Range and Inclination - DM Height = 800 km

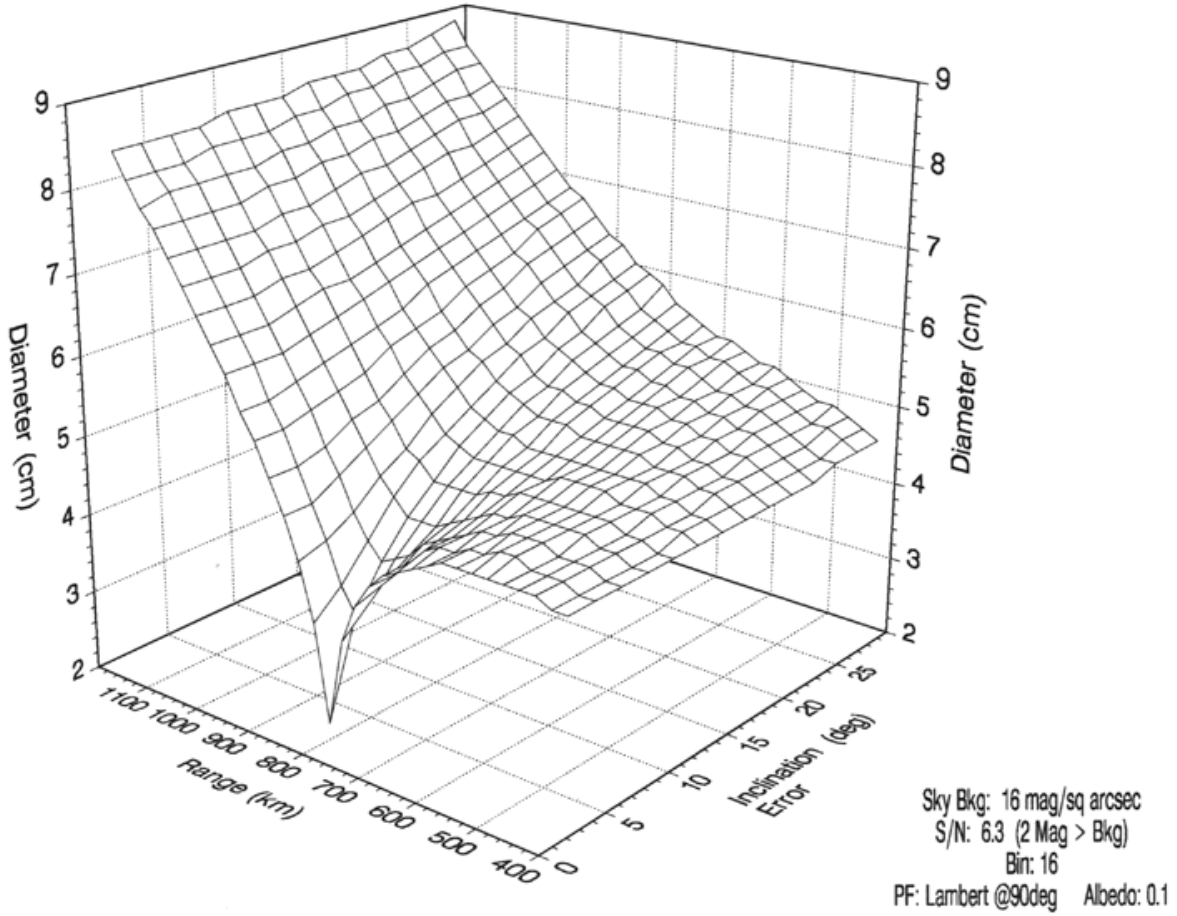

Figure II.B-2. Same DM mode height as in the previous figure (II.B-1) except plotted in terms of limiting diameter. The object is assumed to be a 0.1 albedo Lambertian sphere observed at a 90 degree phase angle. The NASA-LMT could theoretically detect a 2.5 cm diameter object of this type at an 800 km altitude from the JSC location.

NASA-LMT @ NODO: Limiting Detection Magnitude versus Range and Inclination - DM Height = 800 km

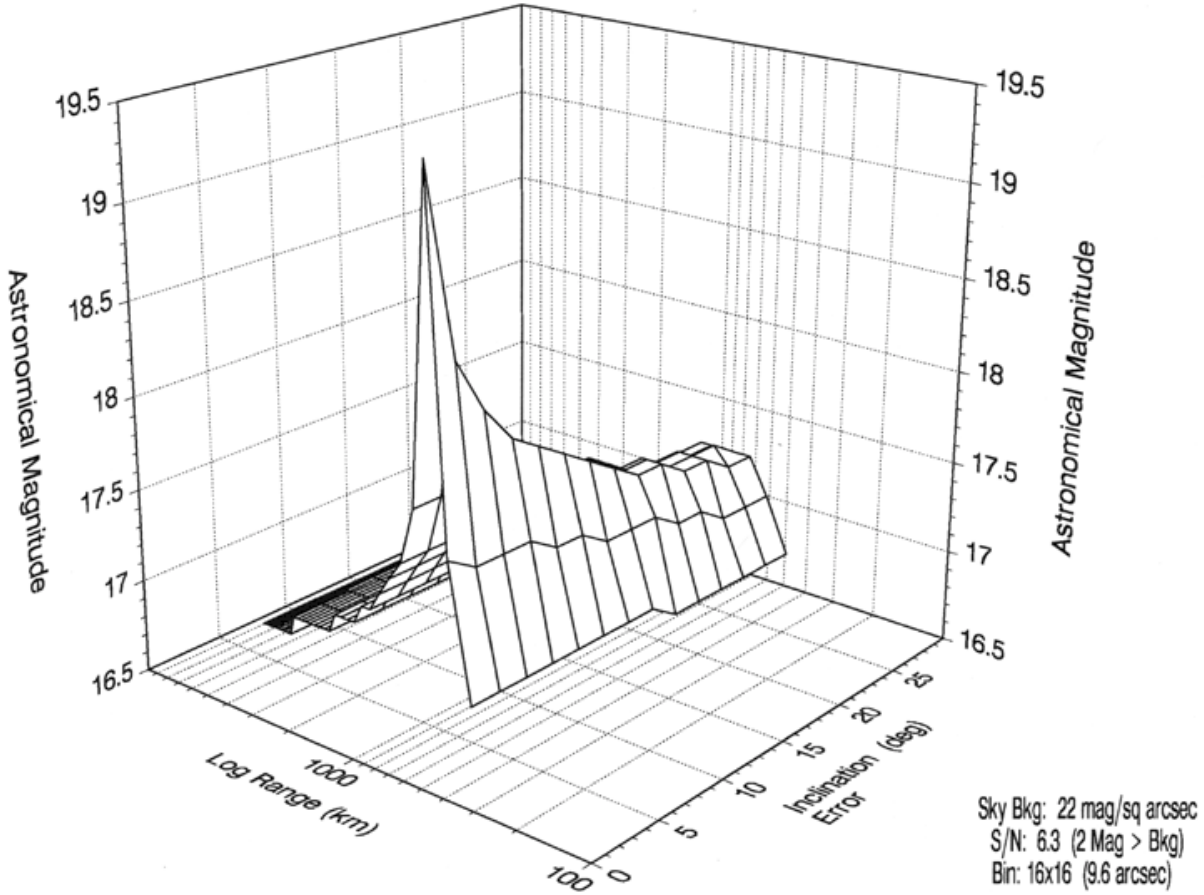

Figure II.B-3. Same DM mode height as in the previous figures except plotted in terms of limiting magnitude for the NODO location with its lower sky brightness (22.0 mag/arcsec ^{2}). A limiting magnitude of approximately 19.5 is reached as opposed to 16.5 at the JSC location. Upon inspection it is apparent that DM mode sensitivity is more tolerant of inclination errors than altitude errors.

NASA-LMT @ NODO: Limiting Detection Diameter versus Range and Inclination - DM Height = 800 km

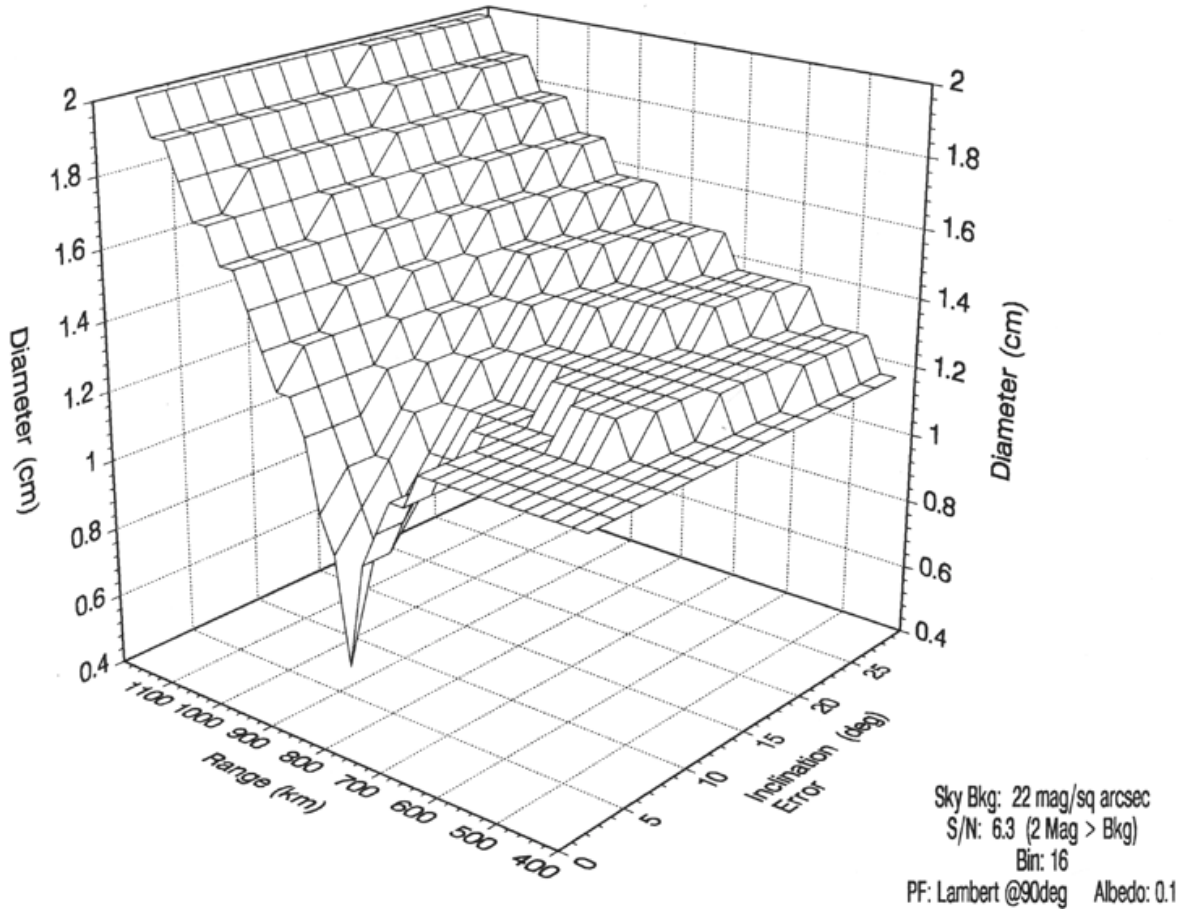

Figure II.B-4. Same DM mode height as in the previous figures except plotted in terms of limiting diameter for the NODO location with its lower sky brightness (22.0 mag/arcsec ^{2}). The object is assumed to be a 0.1 albedo Lambertian sphere observed at a 90 degree phase angle. The NASA-LMT could theoretically detect a 0.8 cm diameter object of this type at an 800 km altitude from the NODO location.

NASA-LMT: Limiting Detection Magnitude versus Range and Inclination – Sidereal Drift Scan

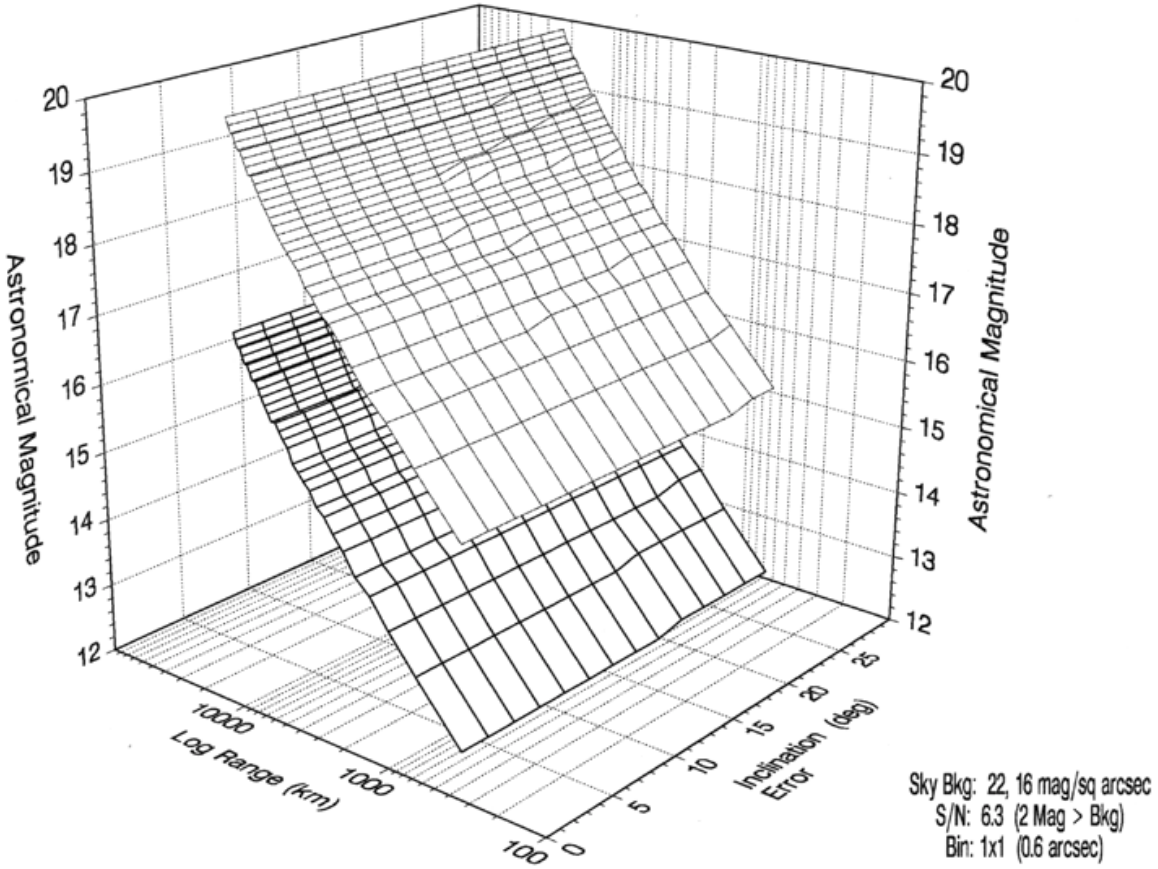

Figure II.B-5. A graph showing the detection sensitivity of the NASA-LMT at two observatory locations while tracking stars in Sidereal Drift Scanning mode. There is a dramatic difference in limiting magnitude between the lower surface with a 16.0 mag/arcsec ^{2} sky background (JSC) and the upper surface with a 22.0 mag/arcsec ^{2} sky background (NODO). Sensitivity for orbital objects is poor at low altitude, but increases rapidly with height as the orbital angular velocity more closely matches the sidereal drift and the effective exposure time therefore increases.

NASA-LMT: Limiting Detection Magnitude versus Range and Inclination – Single Frame 3 & 300 sec Exposures

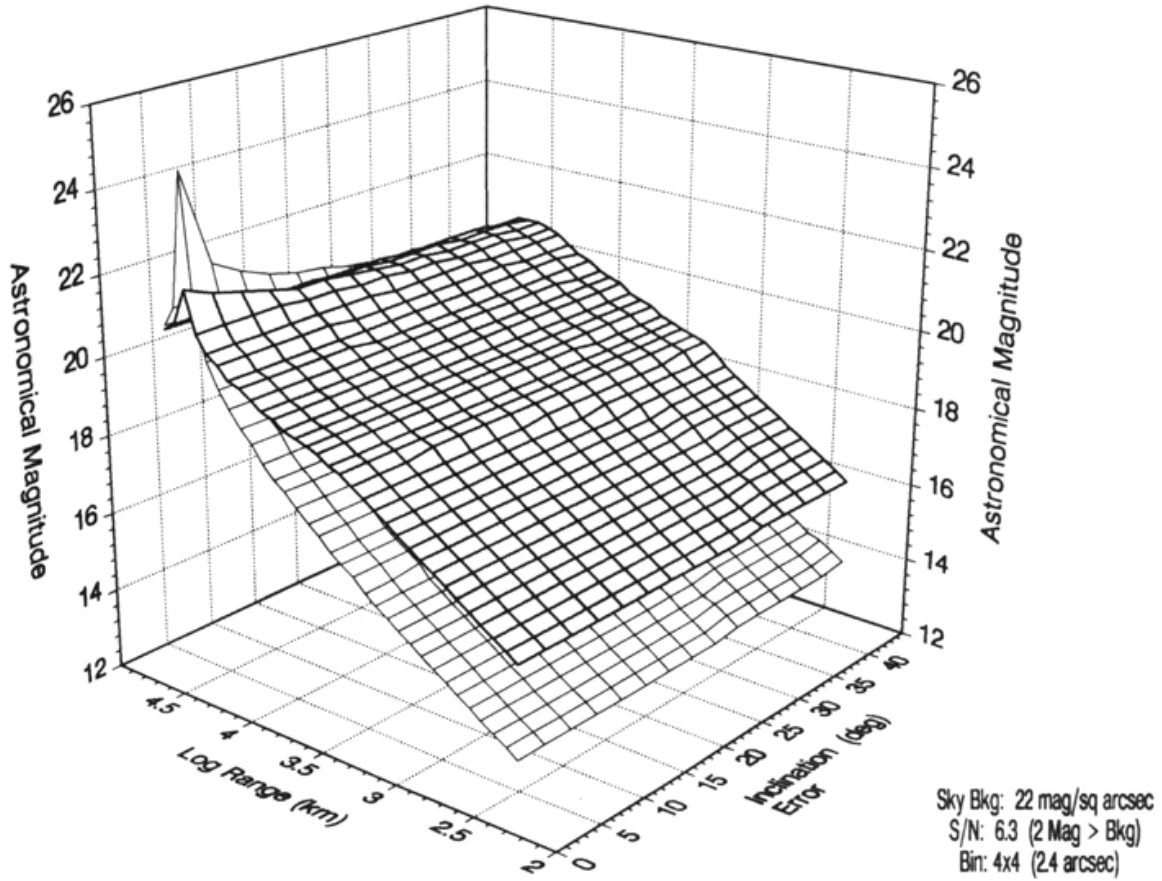

Figure II.B-6. A graph showing the predicted detection sensitivity of the NASA-LMT for the NODO location in a non-TDI single frame exposure mode. The upper and lower surfaces represent 3 and 300 second exposures respectively. With the exception of high altitude objects, which remain quasi-stationary in the FOV, longer exposures result in decreased sensitivity because of the addition of extraneous background noise long after the object of interest has left the FOV.

written to generate these figures).

In actual practice, the sensitivity as measured by the LMT was less than that predicted due to several factors: less than perfect seeing, pincushion distortion in the original corrector that caused the object images to move at a non-constant rate (decelerating towards field center, then re-accelerating away from center), enhanced background noise levels due to smearing of the light from background stars, poor CCD charge-transfer-efficiency (CTE), and the discreet CCD parallel shifting (Hickson and Gibson 1992) relative to the continuous nature of the object motion. Figure II.B-7 shows the results of the DM operating mode in the detection of a catalogued orbital debris object after the LMT was fully operational in 1995. Using this example as a fiduciary, the NASA-LMT limiting detection diameter is approximately 2.5 cm rather than the ~1 cm predicted at this 1117 km altitude. Note the image blur and the enhanced and uneven background levels caused by field stars. Additional examples are shown in Chapter VI.

Because of these additional factors, and the highly selective nature of the DM technique, a suite of image-intensified detectors eventually supplanted the CCD detector for orbital debris data acquisition despite their intrinsically higher noise levels and lack of TDI capability. The image-intensified detector presently employed is limited to reliable detection of objects approximately 3 cm diameter or larger, but its sensitivity is independent of object PA and only weakly dependent on rate so the event rate is much higher. Examples of image-intensified orbital object detection are shown in Chapter VI.

Having arrived at the basic specification for the new LMT, engineering development began in early 1991 with experimental work on a 1meter diameter f/1

Orbital Object Detection via CCD Drift-Matching Mode

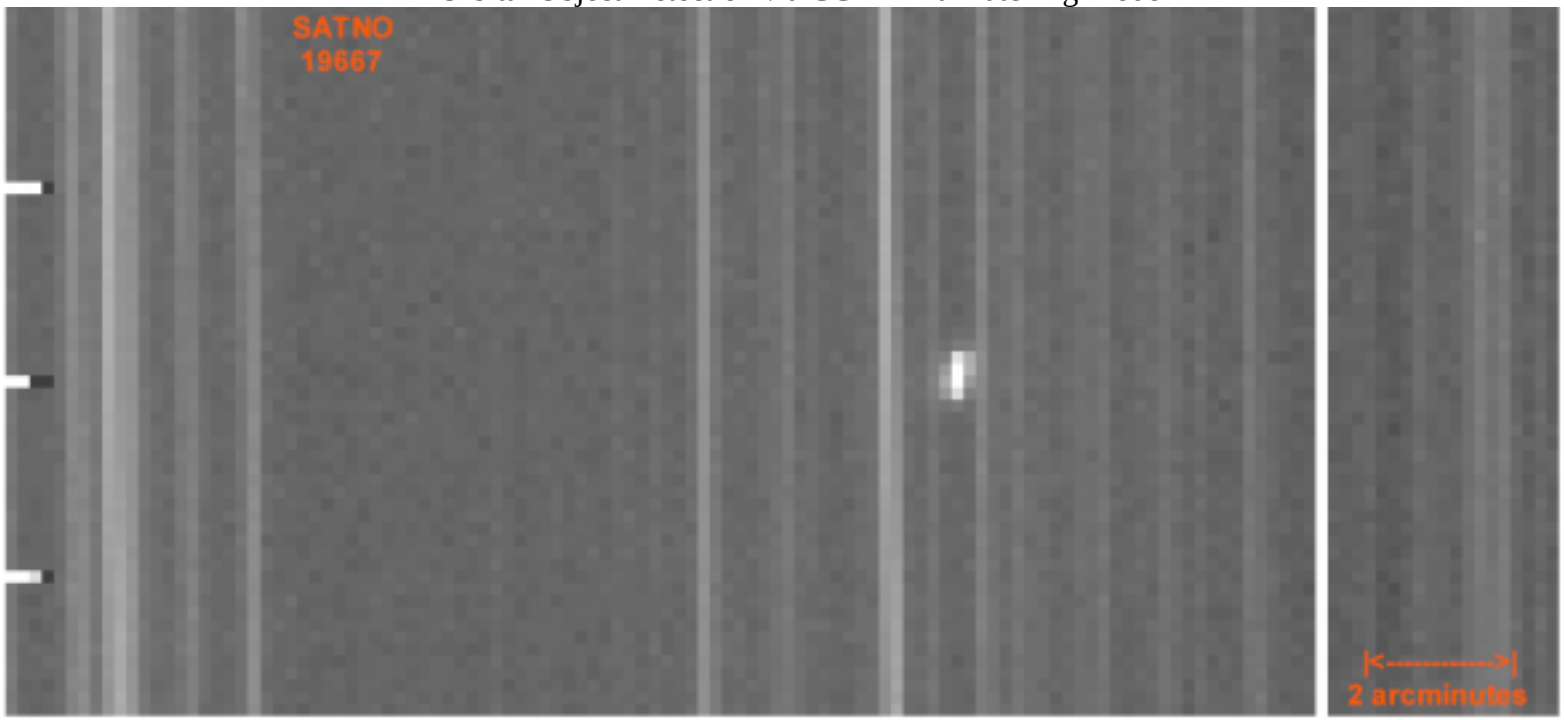

Figure II.B-7. A demonstration of the detection of an orbiting object via the drift-matching mode of CCD operation. The CCD has been set such that its read direction and read rate exactly match the orbital parameters of a catalogued object. In this example, the object is Satellite Number 19667 which is a piece of Thorad Agena debris with a RCS derived diameter of 12.1 cm. When crossing through the LMT FOV, the object was at an altitude of 1117 km with an angular velocity of 0.374 degrees/sec, and a position angle of motion of 255 degrees. The CCD was oriented accordingly and then read at the corresponding rate. The object signal photons were then able to accumulate on only several pixels rather than streak through the FOV. The vertical streaks are background stars which are virtually stationary at this high read rate and short effective exposure time of 0.912 seconds. Based upon the measured net flux above background (2312 ADU) coupled with the assumption of a 0.1 albedo and a specular phase function, the object optical cross-section (OCS) based diameter is approximately 6.52 cm. The limiting detection diameter (at a SN ratio of 6.3) implied by this example is approximately 2.5 cm. This white light image was acquired with the LSP 2K CCD with 16x16 binning in order to accommodate the high angular rate and consequent short readout time.

prototype mirror that was used to test basic concepts. The performance of air bearings, drive motors and electronics, mirror designs, spin-casting techniques and materials, and preliminary optical properties via radius of curvature Focault knife-edge testing were all investigated.

Beginning from a relatively simple conception of the system requirements, the engineering team gradually became aware of the complexities associated with producing an operating telescope. Of primary concern was the performance of the original Warren Machining air bearing which would serve as the rotating platform for the liquid mirror. After repeated modifications by the manufacturer, the bearing was able to support the anticipated mirror container and mercury load (450 kg) while rotating freely, but the angular moment stiffness was only marginally better than the critical value (Chapter IV). Since funding was limited and the bearing was ostensibly adequate, it was retained when development began on the 3m mirror. Only later, after the 3 m container was installed, did the air bearing exhibit an oscillatory instability (air hammer) under variable angular load that made it wholly unsuitable. An alternate bearing from Professional Instruments (described more fully in Chapter IV) rescued the project from termination. Figure II.B-8 shows the Warren bearing during preliminary axial load testing.

Despite the problems regarding the first air bearing, development of the 1m prototype was always instructive and several systems were retained for use with the 3.0 m mirror. The original Lockheed Project Engineer, Terry Byers, who was responsible for most of the early investigations, designed and implemented a motor controller system that was retained for the 3 m mirror and used during the first three years of operations

Prototype 1.0 meter LMT - Warren Air Bearing Load Testing

Figure II.B-8. View inside NASA-JSC building 268 showing the prototype air bearing involved in an axial load test. The Warren air bearing has been axially loaded with 545 kg of lead bricks, thus duplicating the anticipated load of the 3.0 m mirror (160 kg) and a maximum 4 mm thick layer of Hg (390 kg). A suitable air bearing must satisfy both axial and angular load capacity criteria, but in this test, the bearing could not sustain the load without binding during rotation. Modifications were later made which enabled the bearing to successfully support a 680 kg load. The bearing was also able to meet the angular load capacity criteria (Chapter IV), but ultimately failed due to an oscillatory instability. The bearing was replaced with the completely successful PICo air bearing. Engineer Frank Gibbons, the original Lockheed Project Manager, is in the background with the drive electronics at his left.

(1994-1996). Although it was ultimately replaced with a commercially available controller (Chapter IV), it is still used as a backup today. The 12-pole brushless DC 3-phase direct drive motor that Byers selected is still used exclusively and it has also been employed in the 6 m LZT (Hickson PC). Based upon the experiences with the NASA-LMT, the direct drive method has supplanted the belt drive in all new LMT designs.

The 3 point I-Beam base which provides the adjustable interface between the air bearing and the pier and thereby supports the entire mirror assembly, was also retained from the 1 m prototype. A monolithic design was developed at NODO but has not yet been implemented. In the interim, the base was stiffened in 1996 with additional welds, and the original 3-point leveling system, utilizing modest 0.8 cm diameter jack screws, was replaced with 2.54 cm diameter jack screws with 40 threads per inch. These engage the pier via 2.54 cm diameter gauge balls and lapped cups and pads. These modifications improved the ability to level the assembly to sub-arcsecond accuracy, and reduced its flexure, which previously had only marginally satisfied the compliance criteria.

The rudiments of the compressed air system employed for the 1 m prototype were retained for the 3 m mirror and then significantly expanded upon during subsequent operations. A complete revision was performed in early 1996 after moisture condensed inside the PICo air bearing during exceptionally cold conditions at NODO. The air bearing had to be returned to the vendor to be rebuilt because the condensate had deposited a precipitate (emanating from the consumable desiccant in the air dryer) in the fine compensating grooves internal to the bearing. The air system now employs a membrane dryer yielding an output flow at a maximum $-32\,^{0}C$ dew point (Chapter IV).

The 1 m mirror container consisted of a commercially available satellite dish. While adequate for this small size, the thin-walled fiberglass construction was not adequate for supporting a 3.0 meter diameter Hg layer either because of excess flexure or the possibility of structural failure. Rather than attempt a mirror container development effort, it was deemed prudent to retain Hickson to fabricate the 3.0 m primary mirror container. At the time the NASA contract was initiated in May, 1992, Hickson had already constructed two 2.7m diameter liquid mirror containers – one for his own UBC/Laval LMT, and one for the UWO LIDAR (both described in Chapter I).

The epoxy spin-casting trials conducted with the 1 m prototype provided indispensable practice for the 3 m mirror. Epoxy was ultimately rejected in favor of polyurethane for the spin-cast medium due to its lower coefficient of thermal expansion (CTE), but the time critical aspects of mixing resin and catalyst, and the method of pouring the liquid polymer onto the bare mirror surface with minimal air entrapment were identical. Since the spin-casting process could not be easily repeated if mistakes were made, prior experience was important. Figure II.B-9 shows the 1 m prototype with a freshly spun-cast epoxy surface.

Although the liquid mirror surface was already known to be globally parabolic, the extent to which environmental factors such as vibrations, wind, or convection, might affect the localized mirror surface quality was a subject of concern. Following Borra's rigorous optical tests of laboratory liquid mirrors, less rigorous, qualitative tests were planned for the 1m and ultimately the 3m mirrors in an observatory environment. Similarly, although the effects of angular velocity instability, or misalignment of the

NASA-LMT: Prototype 1.0 meter LMT

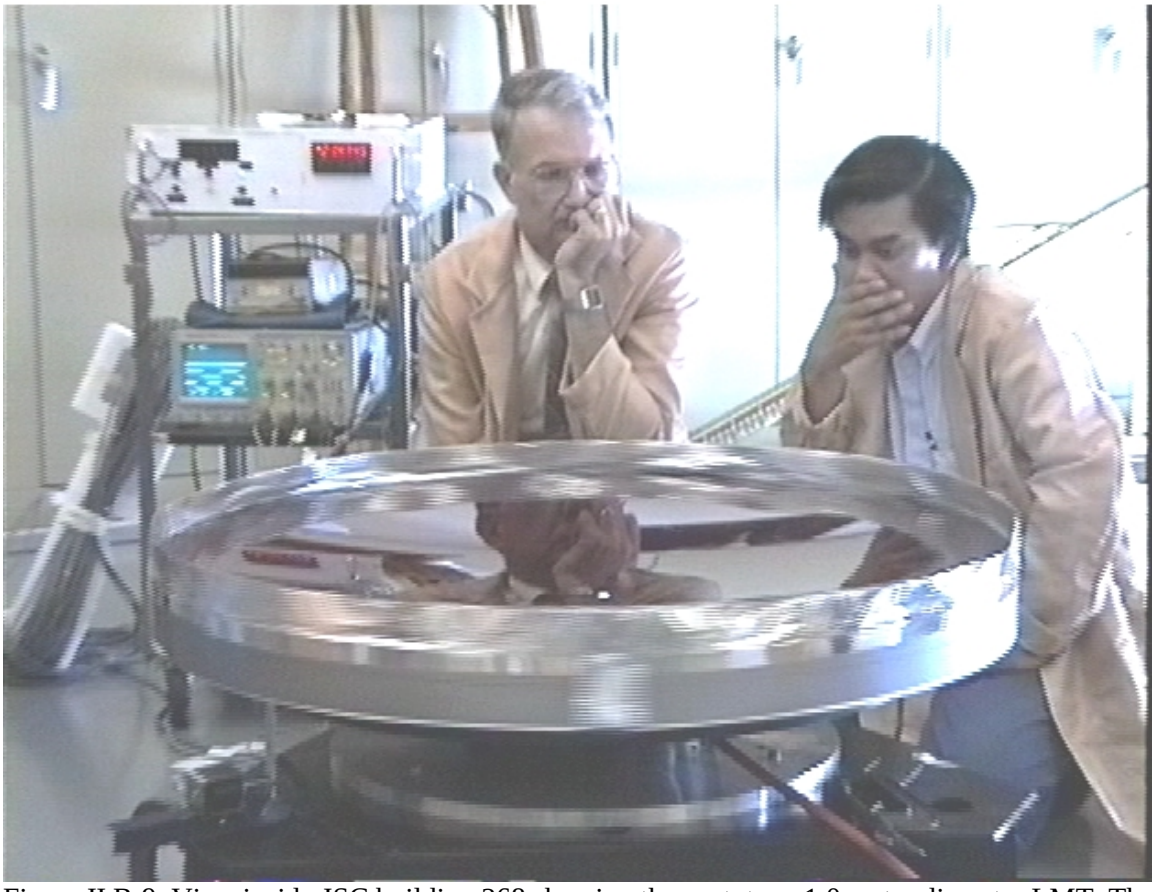

Figure II.B-9. View inside JSC building 268 showing the prototype 1.0 meter diameter LMT. The spun-cast epoxy surface is visible. The rack in the background contains the motor drive electronics and an oscilloscope displaying both the drive input and the output from an encoder on the mirror axis. The two are synchronized. The LED tachometer display reads 21.16 RPM corresponding to a 1 meter focal length. Original Project Engineer Terry Byers is at center, his assistant Andy Wyn is to his left.

rotational axis with the local gravitational field, had been addressed theoretically by Hickson and empirically by Borra, an exploration of these effects on the NASA instruments was deemed prudent in order to gain firsthand familiarity with the various manifestations on the optical surface. To this end, a platform was erected above the 1 m mirror to enable Focault knife-edge and Ronchi testing of the mirror surface under point-source illumination at the radius of curvature. Rather than contend with Hg for the preliminary tests, liquid water was employed as a partially reflective medium. The test setup and a sample image (and its inverse) are shown in Figures II.B-10 through 12.

The tests revealed the presence of the spiral-shaped waves that were first noticed by Borra. These waves were also observed later during NASA-JSC and NODO testing of the 3m mirror with a Hg surface. They are ever-present and independent of any external environmental factors such as vibration, wind-loading, or convection, or any mechanical factors such as angular velocity stability or mirror tilt. They are the dominant defect visible on the mirror surface and appear to be intrinsic to the rotating system - possibly due to an interaction between the mirror liquid surface and the air immediately above the mirror as discussed more fully in Chapter III.

During the middle to latter stages of 1m prototype testing in 1991-1992, procurement began of the various components to be used with the 3m liquid mirror. These included the CCD camera and control computer, the corrective optics, the prime focus motion stages and support legs, and of course the 3.0 m primary mirror container along with 35 liters of triple-distilled Hg – an amount sufficient to generate a 5mm Hg layer if necessary. A relatively inexpensive grain silo was erected at NASA-JSC to

NASA-LMT: Prototype 1.0 meter LMT

Figure IIB-10. View inside JSC building 268 showing the prototype 1.0 meter diameter LMT. This image was acquired after a spin-casting trial with epoxy in which excess air entrapment occurred. The scaffold enabled access to the mirror's radius of curvature for Focault testing of the mirror's figure. The nitrogen bottle in the foreground provided backup in the event of an air system failure. NASA Branch Chief Drew Potter, the initiator of the project, is at left.

NASA-LMT: Prototype 1.0 meter LMT Focault Test

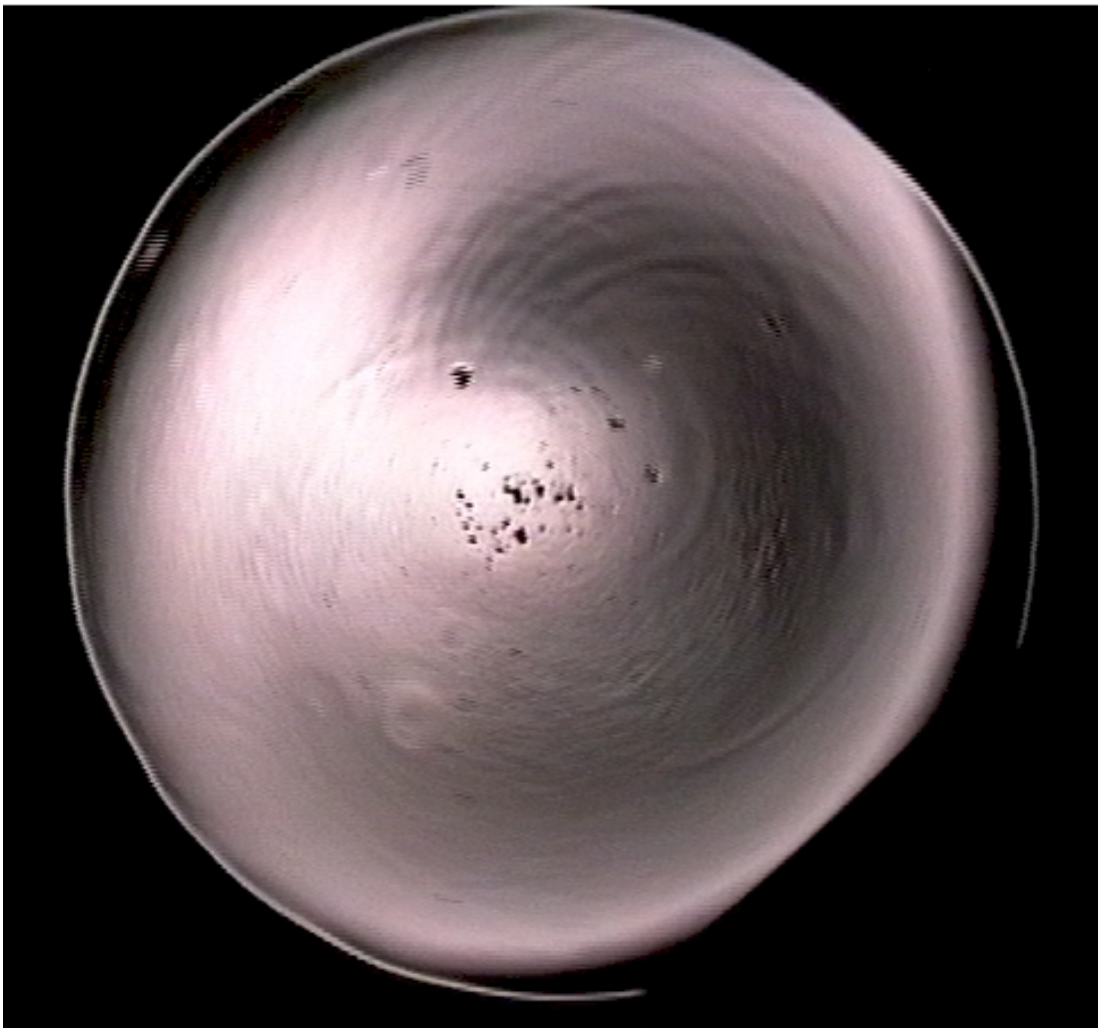

Figure IIB-11. View under point source illumination and knife-edge of the prototype 1.0 meter diameter LMT using liquid water as a reflective medium. The mirror shows the characteristic donut pattern of a parabolic surface figure. Spiral waves (also seen on the final 3 m LMT (Chapter III)) are visible spanning the center to mirror edge. Small circular features are defects in the epoxy. The mirror has a 1 meter focal length and is spinning at angular velocity (ω) of 2.216 rad/sec in the counter-clockwise (CCW) direction.

NASA-LMT: Prototype 1.0 meter LMT Focault Test

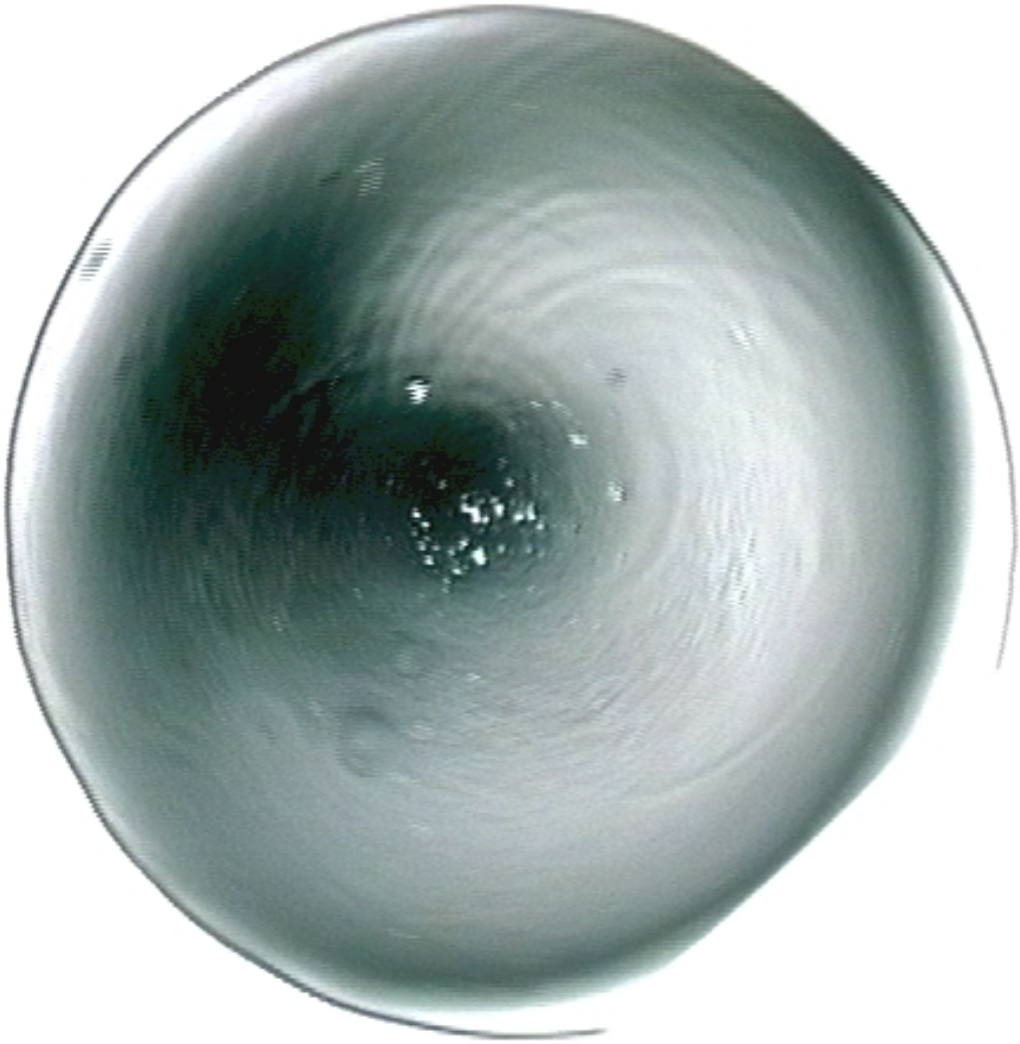

Figure II.B-12. View under point source illumination and knife-edge of the prototype 1.0 meter diameter LMT using liquid water as a reflective medium. This is the same image as in Figure II.B-11 except inverted to show the continuation of the spiral wave pattern.

serve as the observatory building during initial tests. The building was 7.3 m in diameter and 12.2 m tall to help shield the liquid mirror from external winds and enable access to the mirror radius of curvature for optical testing. It was built around a vibration isolated 1 m thick monolithic concrete pier upon which the mirror and prime focus support legs would rest. The silo roof was modified by the manufacturer with a 3.4 m diameter aperture to enable celestial observations at zenith. This aperture was covered with a polyethylene pool cover which was removable for nightly tests via an interior scaffold which also enabled access to the prime focus array and the radius of curvature. Figure II.B-13 shows the exterior of the observatory silo. Figures II.B-14 and 15 show some of the mirror- related system components assembled in the silo prior to installation of the interior scaffolding and a simple block diagram illustrating the system layout. The air compressor (not shown) was on a separate pad isolated from the silo in a small shed at 15 m distance.

The 2048x2048 square array 15 um pixel CCD was made available free of charge by NASA-Goddard as part of a Ford Aerospace foundry run initiated by Lick and Smithsonian Astrophysical Observatories and Photometrics Limited (LSP) (Tritsch PC). The LSP 2K CCD was integrated into a thermo-electrically cooled camera head by Photometrics Ltd. and then supplied to NASA as a turn-key system with a SUN Microsystems Sparc IPC computer and 2GB of disk storage (Figure I-5). The LSP 2K CCD was intended for relatively high-speed (500 kHz) operation for LEO-DM observations and as such possessed high read noise (28.1 electron/pixel) and only a 12-bit A/D converter rather than 16-bit, thus limiting its dynamic range to 4096 ADU (analog-

NASA-LMT: JSC Silo

Figure II.B-13. Exterior view of the grain silo used as the testing facility for the NASA-LMT at the Johnson Space Center, Houston, TX. The 7.3 m diameter by 12.2 m tall structure had a removable 3.4 m diameter ceiling aperture which was covered with a removable polyethylene coated tarp. This cover was manually removed for nightly observations. The silo was sufficiently tall to provide the mirror with partial protection from exterior winds and enable interior access to the radius of curvature. The silo still remains at NASA-JSC where it is used for storage.

NASA-LMT: Developmental LMT System within the JSC Silo

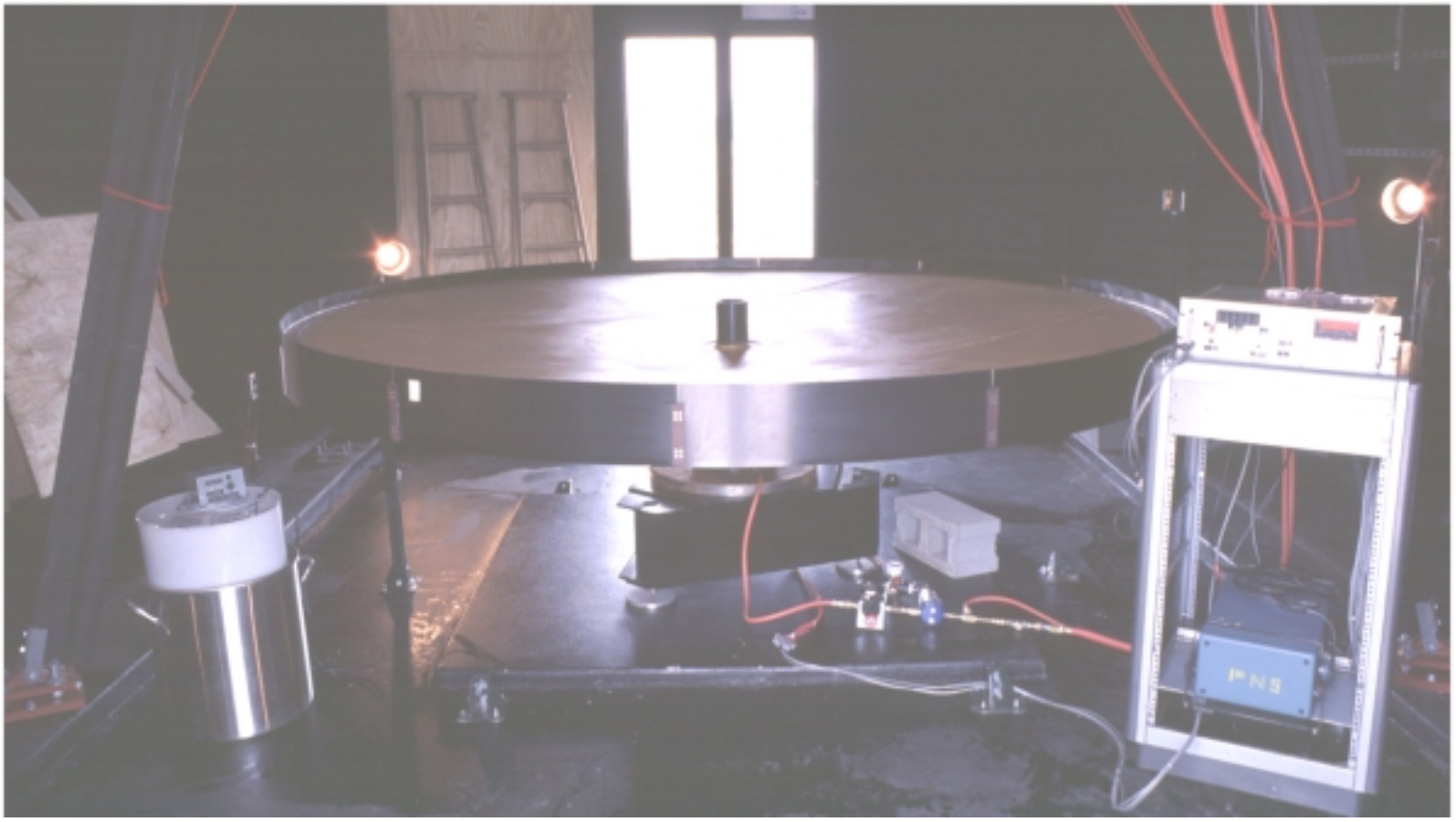

Figure II.B-14. View inside the JSC Silo of the developmental LMT system prior to spin-casting. The prime focus support tripod is installed around the mirror. The Hg storage reservoir is visible at left and the motor control electronics are in the rack at right. A portion of the rudimentary air system is visible beneath the mirror as is the I-Beam base with the Warren air bearing installed.

NASA-LMT: 3.0 m Block Diagram

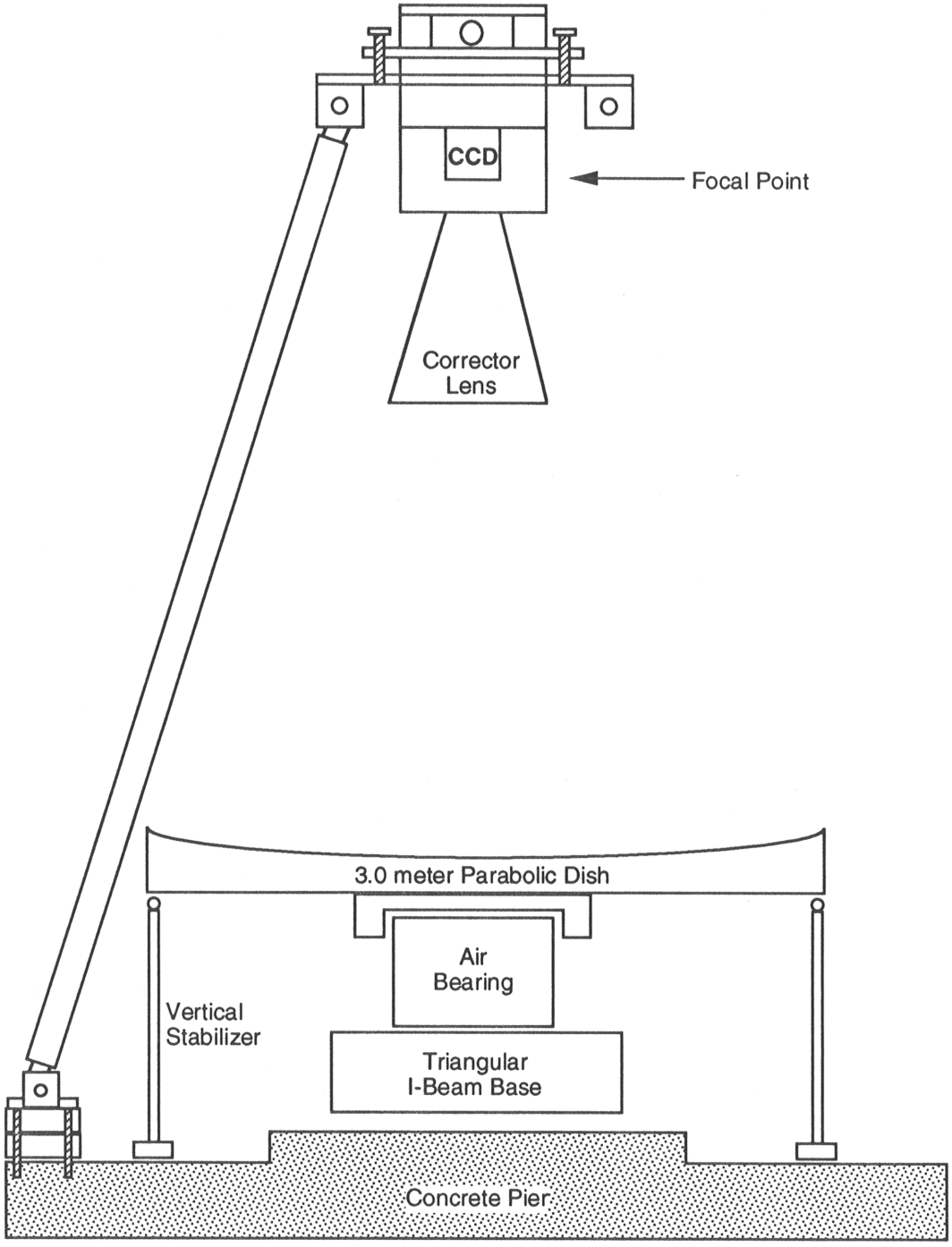

Figure II.B-15. A simple illustration (not to scale) of the organization of components within the 3.0 m LMT system. The vertical stabilizer prevents the mirror from catastrophic tilt.

to-digital units). Despite the limitations, the LSP 2K CCD was perfectly suitable for testing purposes and produced useful astronomical and orbital object detection results as demonstrated in Chapter V. The LSP 2K CCD was used until its failure in the fall of 1997, when it was replaced with a more sensitive back-side illuminated 1024x1024 array 24 um pixel SITe CCD made by Pixel Vision (PV) and loaned to NASA by Paul Hickson and UBC. The data acquisition computer was similarly updated to a SUN Ultra 5 with 36 GB of disk space to keep pace with data storage requirements. PV 1K CCD results are fully described in Chapter VI.

If used alone, the 3m f/1.5 primary mirror would produce very poor images of celestial or orbital objects. By their nature, paraboloids are only capable of diffraction-limited performance for objects on the axis of revolution. Images of off-axis objects exhibit the Seidel wave front aberrations coma and astigmatism (Chapter III). These aberrations become more severe with increasing distance from the optical axis or with decreasing focal ratio. At f/10 the deviation between a parabola and a sphere (which exhibits spherical aberration, but neither coma nor astigmatism) is sufficiently small that the aberrations are negligible, but at f/1.5 the aberrations are severe and the telescope cannot be used for wide-field imaging without the addition of corrective optics. For the NASA-LMT several primary mirror focal ratios and corrector designs were considered during the conception phase. The final focal ratio of the primary mirror was based upon the optical results of these early investigations. At f/1.0, the cost-effective corrective optics available did not yield acceptable image quality throughout the FOV. At f/1.5 however, an affordable 3-element corrector with all spherical surfaces and borosilicate

crown glass (BK7) produced excellent image quality over the entire FOV of the LSP 2K CCD. The f/1.5 primary mirror and the 3-element corrector (designed by EHR Optics (Richardson et al. 1982)) were thus selected for the NASA-LMT final configuration. Figures II.B-16 and 17 show spot diagrams generated from ray tracing the optical systems for both the f/1.0 study and the f/1.5 build design. Figure II.B-18 shows the optical layout of the 3-element corrector and Appendix C1 contains the parameter file detailing the corrector construction. The numbers in parenthesis are the actual measured values as constructed by Applied Physics Specialties (APS).

Unfortunately, it was discovered after the NASA-LMT became operational that the original corrector design possessed some residual field distortion. This would have been acceptable for a single framing detector wherein some field distortion is tolerable, but not for a drift-scanning CCD. As mentioned previously, the pincushion (as opposed to barrel) distortion, caused the stars to move along trajectories curved toward the field center. The stars also moved at variable rates - more quickly at the field edge, decelerating toward field center, and then reaccelerating to exit the FOV. For a CCD operating in TDI whose pixels scan at a constant rate and in straight lines, the pincushion distortion results in some blurring of stellar images. For the NASA-LMT the blurring was only a serious problem at the field edges. To remove the distortion the corrector was modified in 1998 by replacing the rear element with a doublet containing an aspherical surface (Richardson PC). The repair was successful and images are now uniform across the entire field. The repair, including sample images, is discussed in detail in Chapter IV.

Precision remotely controllable motion stages were procured from Klinger (now

Spot Diagram: 3 Element Corrector for a f/1.0 Primary Mirror

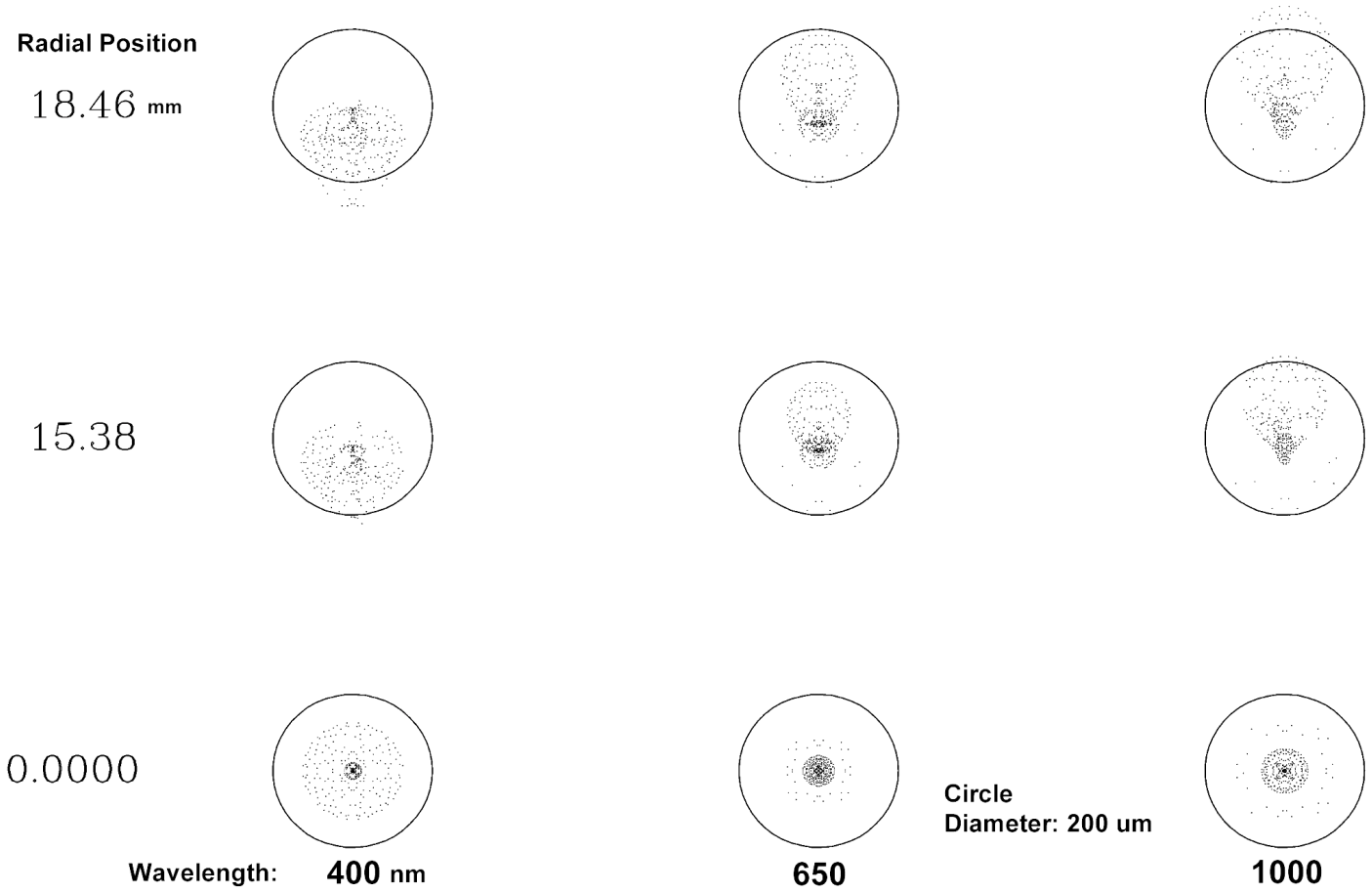

Figure II.B-16. Spot diagram illustrating the optical performance of a 3.0 m f/1.0 telescope fitted with a 3 element corrector. The image quality is significantly diminished at all wavelengths and field positions relative to the f/1.5 design. The reference circles have a 200 um diameter or 13.3 15 um pixels. The best spot at field center and 650 nm has an 80% encircled energy diameter of 3 pixels which equates to 2.7 arcseconds for this design. This is significantly lower resolution than typical seeing limit at NODO and therefore unacceptable. Courtesy E.H. Richardson.

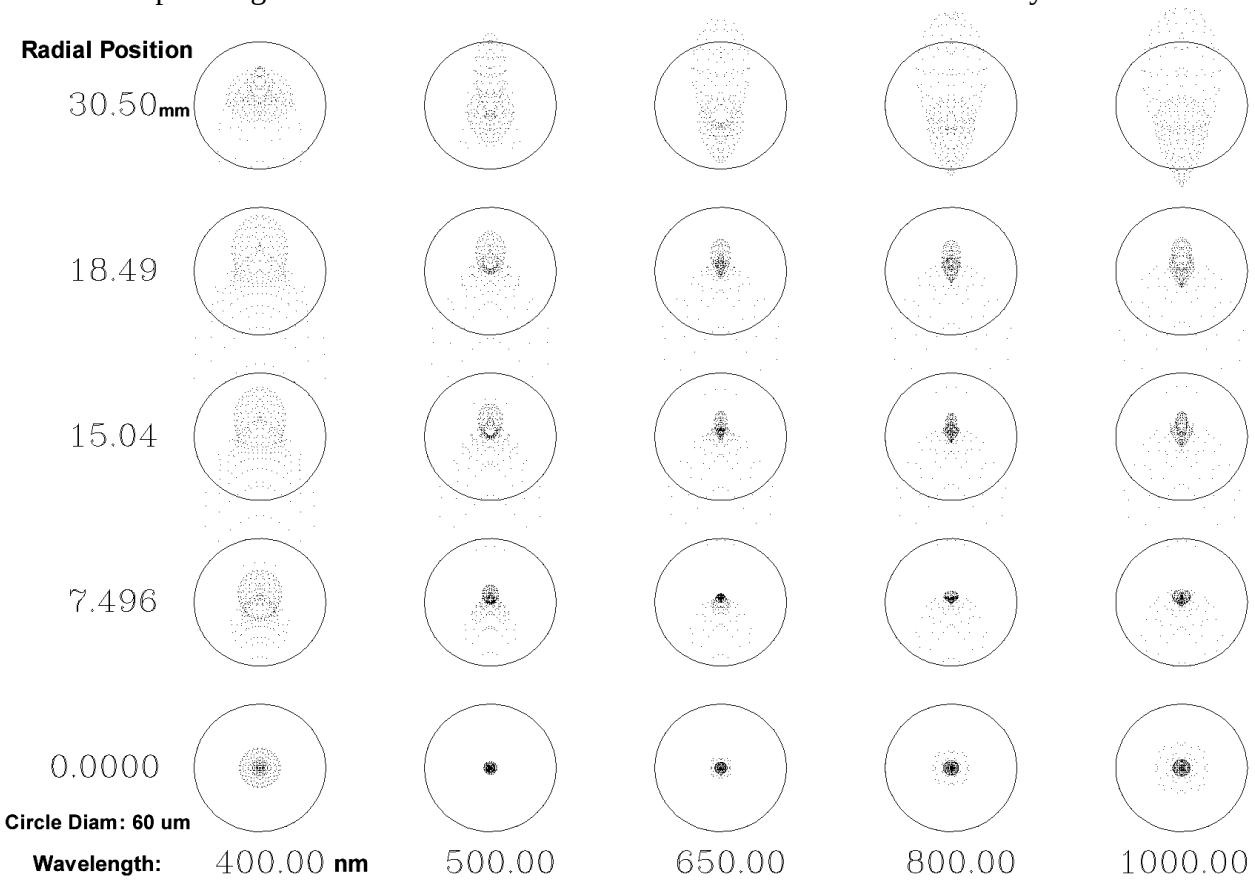

Figure II.B-17. Spot diagram illustrating the optical performance of the 3.0 m f/1.5 NASA-LMT fitted with the chosen 3-element Wynne-type corrector. The circles are 60 um in diameter or 4 pixels on the 15um LSP CCD, equivalent to 2.4 arcseconds (effective focal ratio of f/1.7189). The 80% encircled energy diameters are less than 1.2 arcseconds over the entire field of view of the LSP CCD (<21.7 mm radius) from 500-1000 nm. Furthermore, the 80% encircled energies are less than 0.6 arcsecond (1 pixel) over the central 75% of the LSP CCD FOV enabling seeing limited performance at NODO. Courtesy E.H. Richardson.

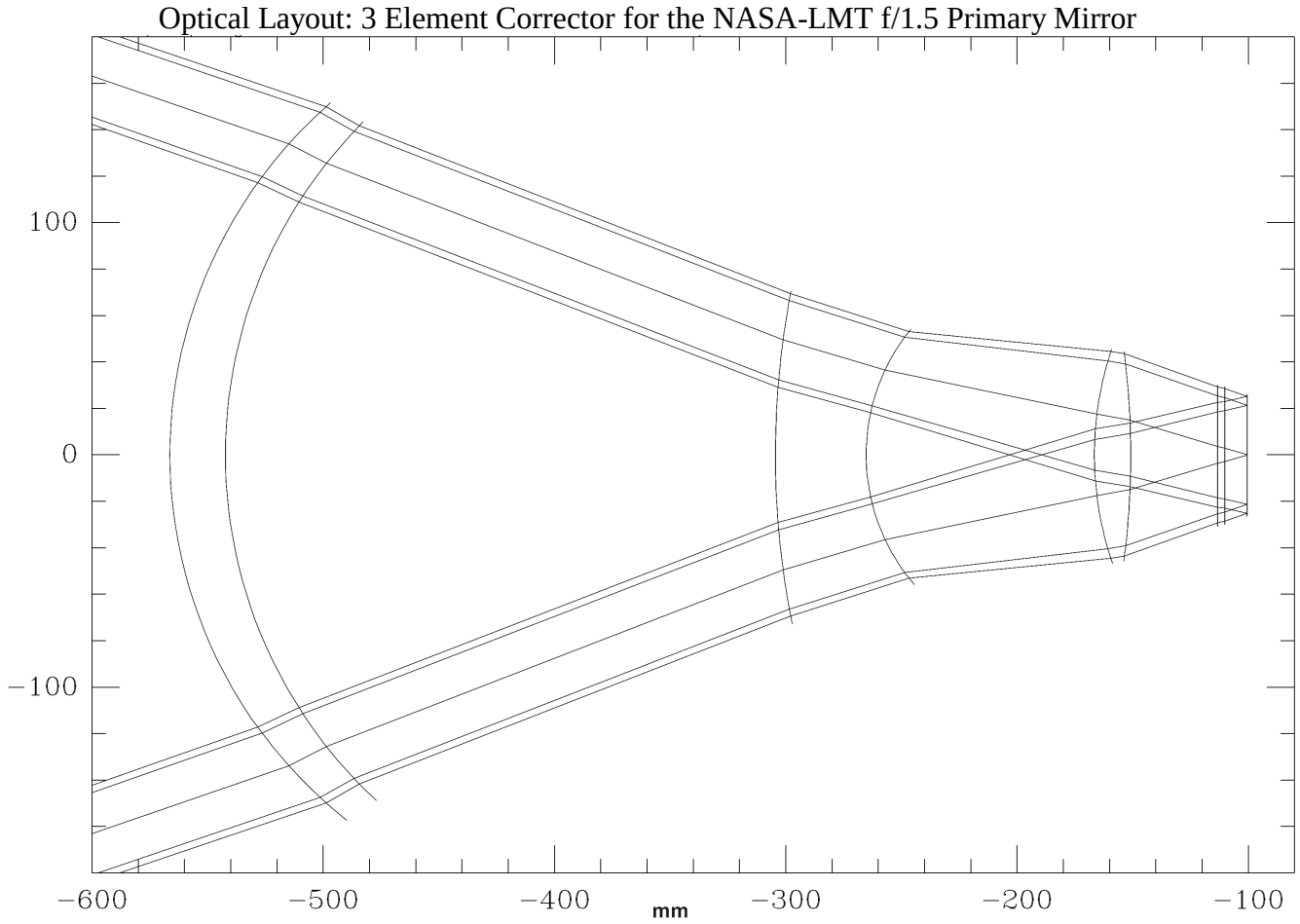

Figure II.B-18. Optical layout of the 3-element Wynne-type corrector for the 3.0 m f/1.5 NASA-LMT. From left to right, the corrector's three spherical BK7 elements are shown, followed by the CCD camera head window and focal plane CCD. All optical surfaces are anti-reflection coated with magnesium-fluoride to improve transmission at each interface to ~98% and reduce internal reflections. Courtesy E.H. Richardson.

Newport Corporation) for accurate positioning of the LSP 2K CCD and the corrector at the prime focus position above the primary mirror. Stages were required for both focus and CCD rotational orientation in order to align the read direction with the sidereal drift of stars or the position angle of motion of orbital objects. Figure II.B-19 shows the original NASA-JSC prime focus configuration of the CCD, corrective optics, and the motion stages above the 3.0 m primary mirror. The focal stage has a range of 9 mm and is capable of $\pm$ 1um vertical resolution. The rotation stage can be aligned to $\pm$ 0.01 degrees which is adequate for proper alignment of the CCD read relative to object motion.

After the 3m components were procured and assembled within the silo, along with a series of rollers beneath the mirror perimeter to protect the air bearing and prevent catastrophic tilting, it remained to spin-cast the polyurethane parabolic substrate and then pour Hg on the mirror. The spincast shown previously in Figure I-9 was performed in May 1993 by the development team with the assistance of Paul Hickson and his assistant Suzanne Watson. Six equal area annuli were drawn on the mirror container surface with each of six people responsible for one annulus. Despite extensive practice with the 1m prototype, the spin-cast was performed twice after excess air was entrapped during the first pour. Air bubbles yield a rough surface which can cause the thin Hg layer to separate, preventing formation of the continuous Hg mirror surface. Surface roughness can also affect a completed Hg surface by printing through to the mirrored surface and consequently degrading image quality. Print through is suspected in the NASA-LMT as described in Chapter V. Tests performed by Hickson (PC) indicate that surface roughness should have a peak-to-peak level of less that one-tenth of the Hg layer thickness. For a

NASA-LMT @ JSC: Prime Focus Array Test-bed

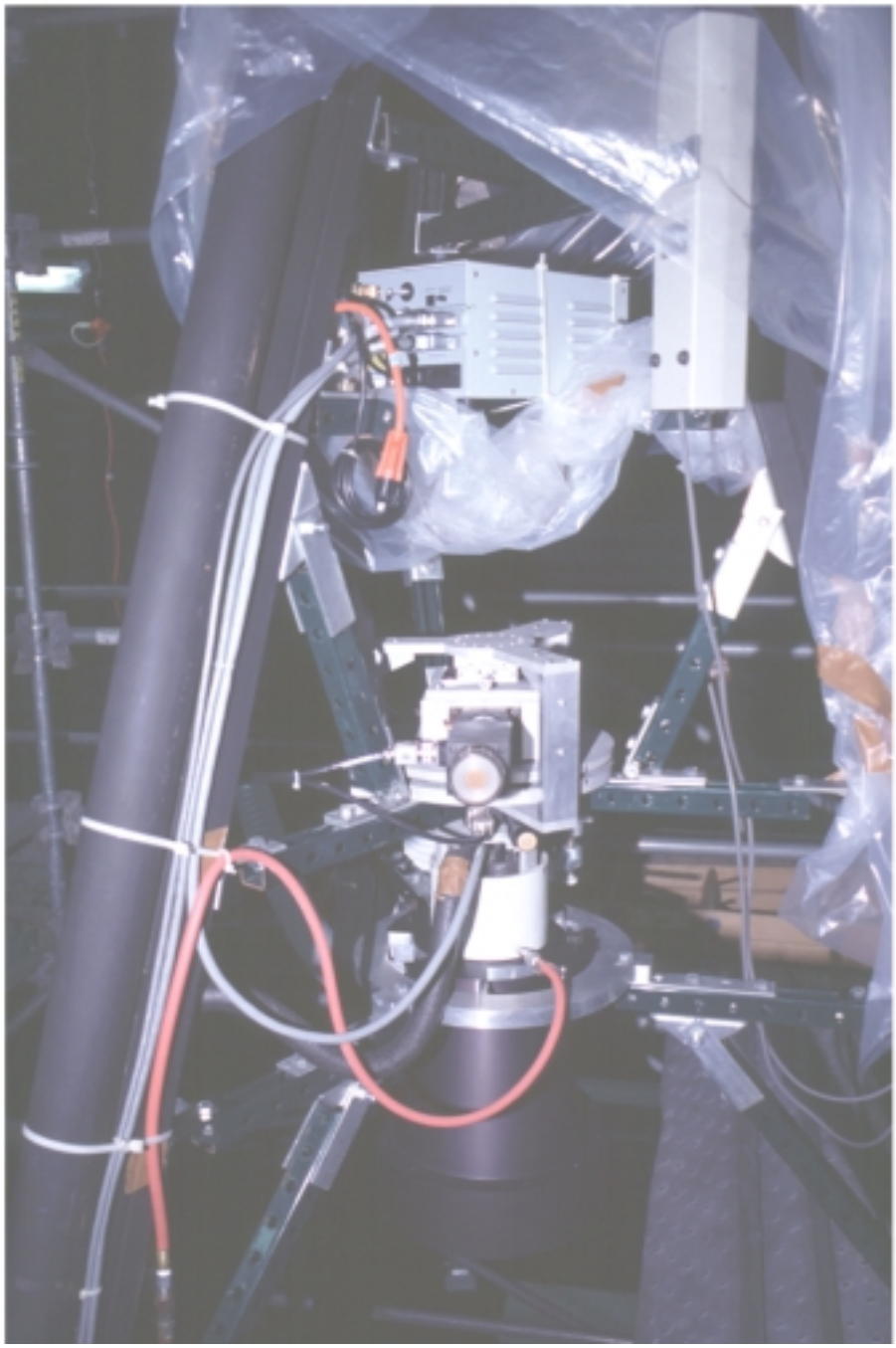

Figure II.B-19. Prime Focus elements of the NASA-LMT within the JSC Silo. This photograph was obtained during early testing of the prime focus components which included the corrector, CCD, and motion stages. The assembly was eventually reconfigured for installation at NODO. Note the red air line used for dew removal from the CCD (inside the white cylindrical cover) and the vertically oriented He-Ne laser (upper right) used for alignment and focal point determination. The CCD control electronics are at top.

1mm thick Hg layer, this implies a maximum deviation for the substrate of 100 um. This was not achieved during the NASA-LMT spin-cast where localized deviations of 0.25 mm exist. The LZT will have a machined and independently adjustable surface enabling the 100 um tolerance to be satisfied.

Approval to fill the mirror with Hg was received from the NASA safety office in November 1993. Approval was subject to the constraint that the mirror be operated at all times with an acetate cover in place. This ultimately proved untenable due to the severe degradation in optical quality and a waiver was eventually obtained. The mirror was initially filled with 25 liters of Hg to yield a 3mm layer after formation. The first spin-up was performed by Paul Hickson who had extensive experience with the UBC/Laval 2.7 m. After 15 minutes effort the largest liquid mirror in existence was formed for the first time at which point it was immediately obvious that there was a problem. The mirror's surface was covered with large amplitude (~ 1 mm) concentric waves accompanied by an audible low frequency hum (~30 Hz). The Warren bearing was exhibiting an oscillatory instability under load known as 'air hammer' in which the supporting air film actually does work on the bearing rotor, thus becoming dissipative of energy in the air stream. Repeated attempts over several weeks failed to improve the oscillation plagued mirror (Figure II.B-20) with the net result that the mirror was useless for astronomical work.

After a 3-year effort, members of the engineering team were needed to work on other projects and NASA was sufficiently frustrated that the LMT project was to be cancelled. With the untimely death of Karl Henize in October 1993, the author's primary project, using the NASA-CDT to observe catalogued orbital objects, was drawing to a

NASA-LMT @ JSC: 3.0 meter LMT with Warren Air Bearing

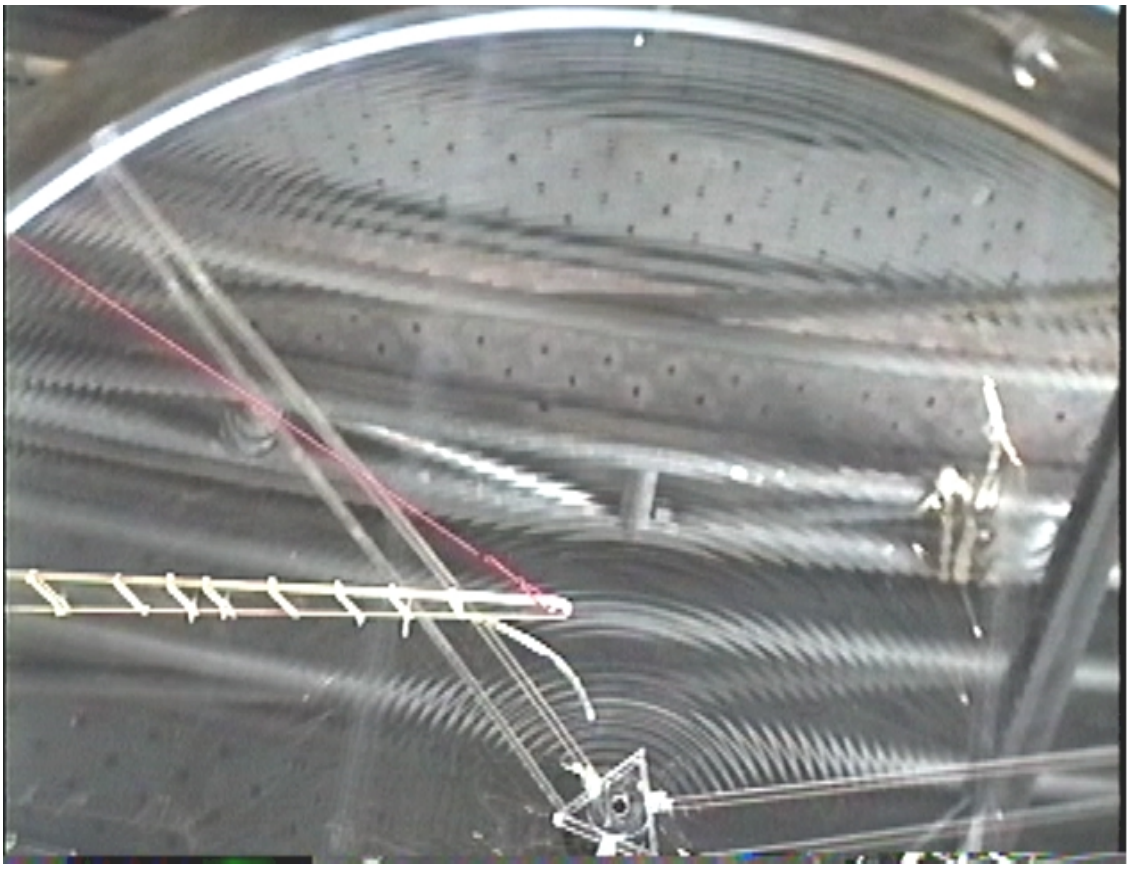

Figure IIB-20. View inside the NASA-JSC Silo showing the 3.0 meter diameter LMT the first day the mirror was filled with Hg and the surface established. The supporting Warren air bearing exhibited an oscillatory instability in which the pressurized supporting air film does work on the bearing rotor, which thereby becomes dissipative of energy in the air stream. Referred to as 'air hammer', this effect rendered the 3m mirror useless for astronomical work by covering the surface with macroscopic concentric waves. The bearing was replaced within three months with one from Professional Instruments which was extremely stable. Note the Hg filler arm which allowed Hg to removed from the mirror after formation to enable thinner Hg layers than could be formed otherwise.

close. Having already helped delineate the scientific objectives and performance specifications, and having procured some of the primary LMT components, the author was assigned by NASA Branch Chief Andrew Potter and Lockheed manager Patrick Jones, the Project Scientist/Engineer role in December 1993.

With the exception of the Warren air bearing, the LMT was basically sound. Even with the inadequate bearing, the mirror/bearing/base system satisfied the minimum angular moment stiffness compliance criteria (Chapter IV). All components were functional including the air system, the direct drive motor and control electronics, and the prime focus assembly consisting of the motion stages, LSP 2K CCD, and the corrector. A review of the available literature for alternate air bearings, assisted by Paul Hickson, indicated that two were available which satisfied the axial load and angular moment stiffness criteria. After lengthy discussions with both vendors Dover and Professional Instruments Company (PICo), it was decided that the PICo bearing offered the best chance of success. PICo chief engineer Gene Dahl, who became instrumental in ensuring the LMT's eventual success, was sufficiently convinced that the air bearing would work that he guaranteed a refund if it failed. With this assurance, NASA was persuaded to provide the additional funds ($20K) for the new air bearing and carriage.

After the new air bearing was installed in February 1994 (Figure II.B-21), progress was rapid with 'first light' being achieved on May 1, 1994. Figure II.B-22 shows the fully operational LMT within the JSC silo and Figure II.B-23 shows the very first image acquired. Although it appears disappointing, it was actually very encouraging. The image shows two bright out-of-focus stars and many faint ones. Each

NASA-LMT @ JSC: PICo Air Bearing Installation

Figure II.B-21. View inside the NASA-JSC Silo showing the installation of the Professional Instruments (PICo) 10R Block-Head air bearing atop the I-Beam base. The bearing and direct drive motor were integrated into a 150 kg package. The bottom hub of the 3.0 meter mirror is visible at the top of the photo. The PICo air bearing enabled the LMT to become fully operational. Frank Gibbons is at left center facing the camera, Terry Byers is at right center, and the author is in the far right foreground.

NASA-LMT: Operational LMT System within the JSC Silo

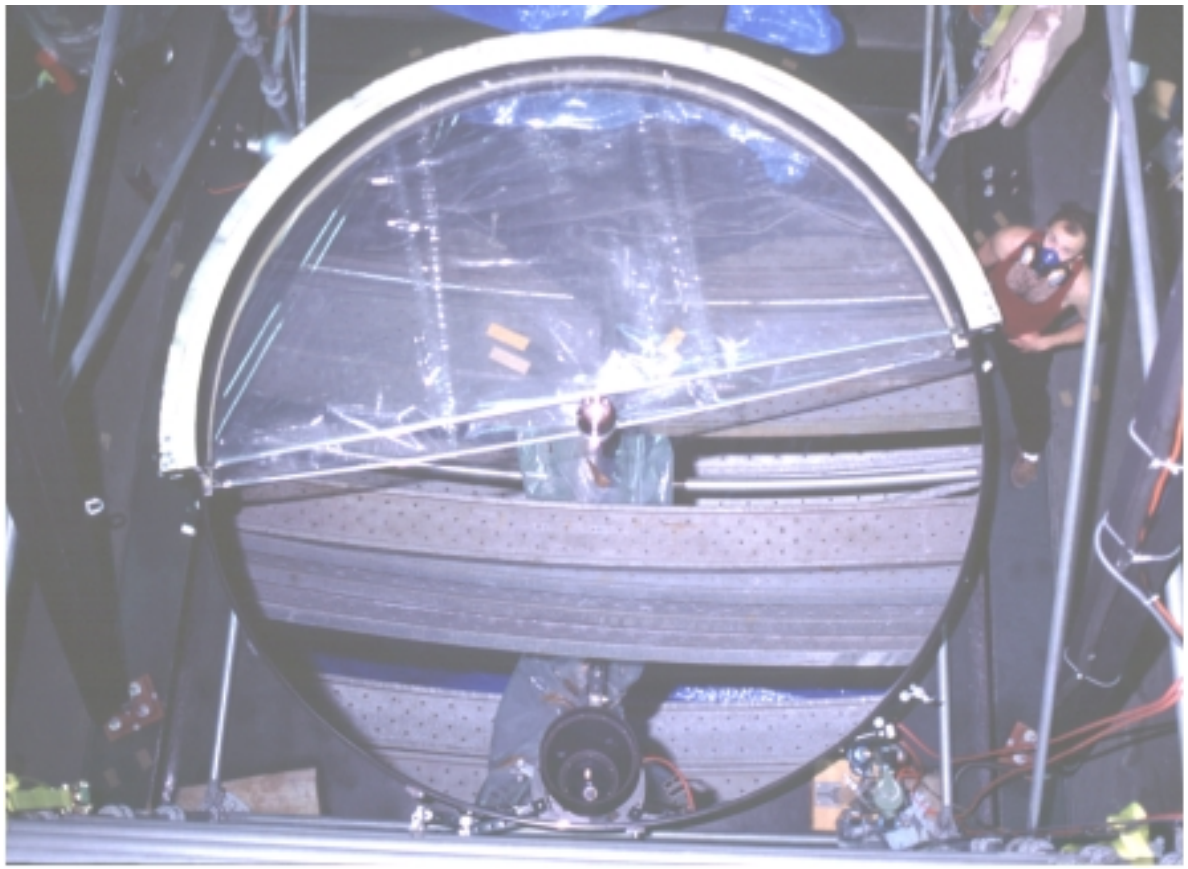

Figure II.B-22. View inside the JSC Silo of the operational LMT system. The mirror is formed and the prime focus array can be seen in reflection. The focal plane CCD is visible centered in the conical corrector lens. The mirror is surrounded by scaffolding which enabled access to prime focus and the silo roof. The mirror is partially obscured by an acetate cover used to inhibit Hg exposure and protect the mirror from debris when not in use. Technical assistant Freeman Bertrand is at right, he played a critical role throughout development and testing at JSC and the first few months at NODO.

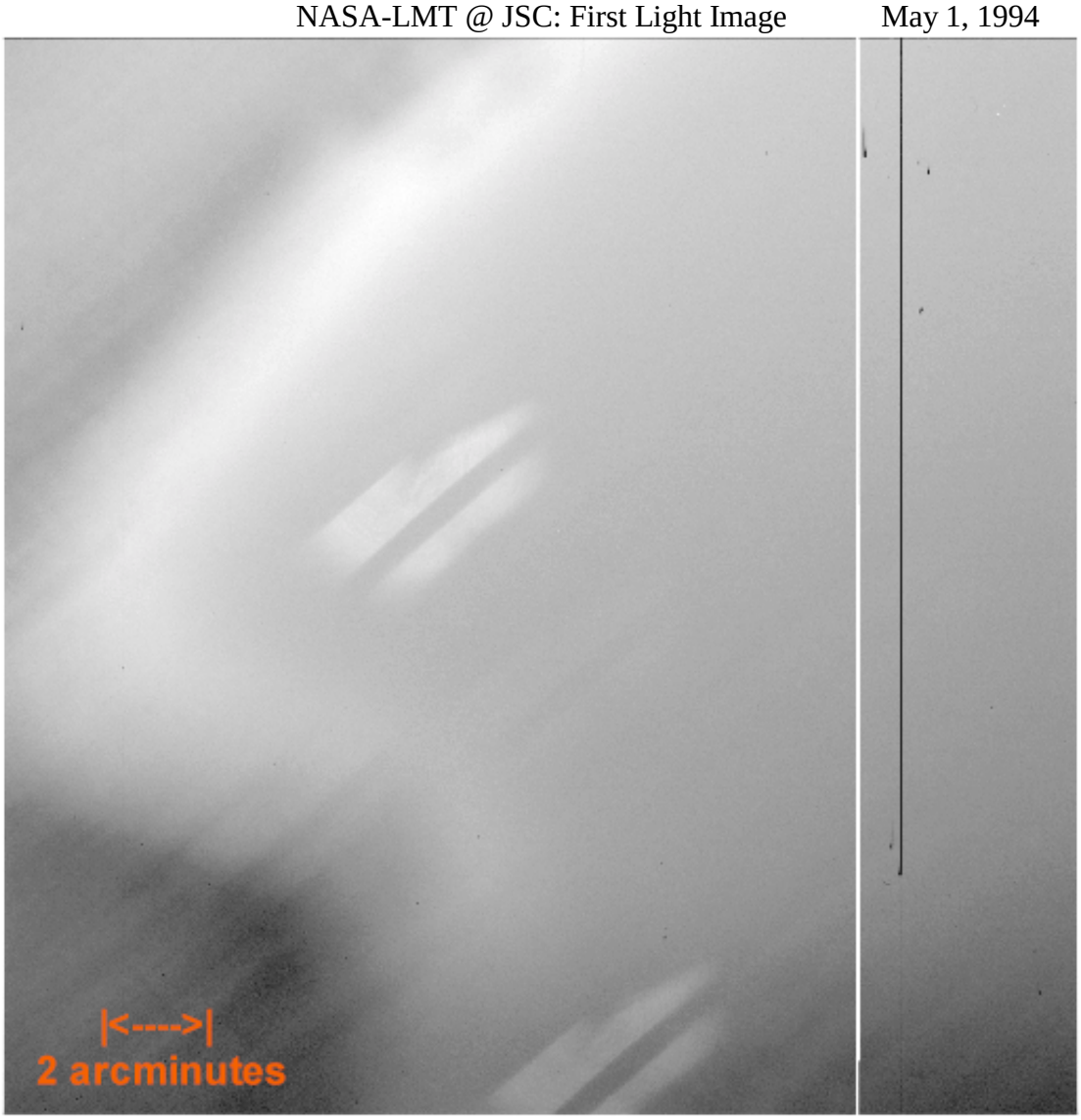

Figure II.B-23. 'First light' image acquired with the 3 m NASA-LMT at NASA-JSC on May 1st, 1994. The image shows two bright out-of-focus stars illuminating the entrance pupil which was partially obscured by the access scaffolding. Many other faint stars are visible in this 2x2 binned white-light image of approximately 90 second exposure time. Binning was used frequently during the initial testing and alignment trials in order to save disk space. The field shows additional obscuration due to the formation of condensation on the camera head CCD window. The high relative humidity in Houston created frequent problems with dew formation. This image offered great promise in the sense that stellar photons were at least reaching the CCD.

stellar image maps the entrance pupil which was 50% obscured with access scaffolding. The field was also obscured with condensation that had formed on the CCD window – a persistent problem with Houston's normally high relative humidity.

Figures II.B-24 and 25 show improvement in the focus and CCD orientation during the first night. The poorly focused star trails in the third image are closely aligned with the CCD read direction, but the read rate does not match the sidereal drift. During the subsequent weeks and months, improvements were made to the prime focus and mirror alignment in an effort to improve the image quality. Figures II.B-26 and 27 show examples of images obtained during the interim stages. The first of these demonstrates the appearance of a sidereal drift scan when the rate is approximately correct, but the rotational orientation of the CCD is misaligned. In this example the stars are drifting orthogonal to the CCD read direction. The first evidence of field distortion appears in this image wherein the distortion causes the S-shaped stellar trails because of the variable angular velocity of stars through the FOV. The second image shows a star field in which image quality is improving, but the images are not yet symmetrical and the resolution is still several arcseconds FWHM.

Figure II.B-28 shows additional improvement and the first detection of extra-galactic objects (three faint galaxies near field center). Figure II.B-29 shows one of the best images obtained at the NASA-JSC location in August 1994. The resolution is a respectable 2.5 arcsecond FWHM. Image quality of this order was sufficient demonstration of the NASA-LMT;s viability that a better location was sought with darker skies, improved atmospheric seeing, and cooler temperatures. The later aspect was

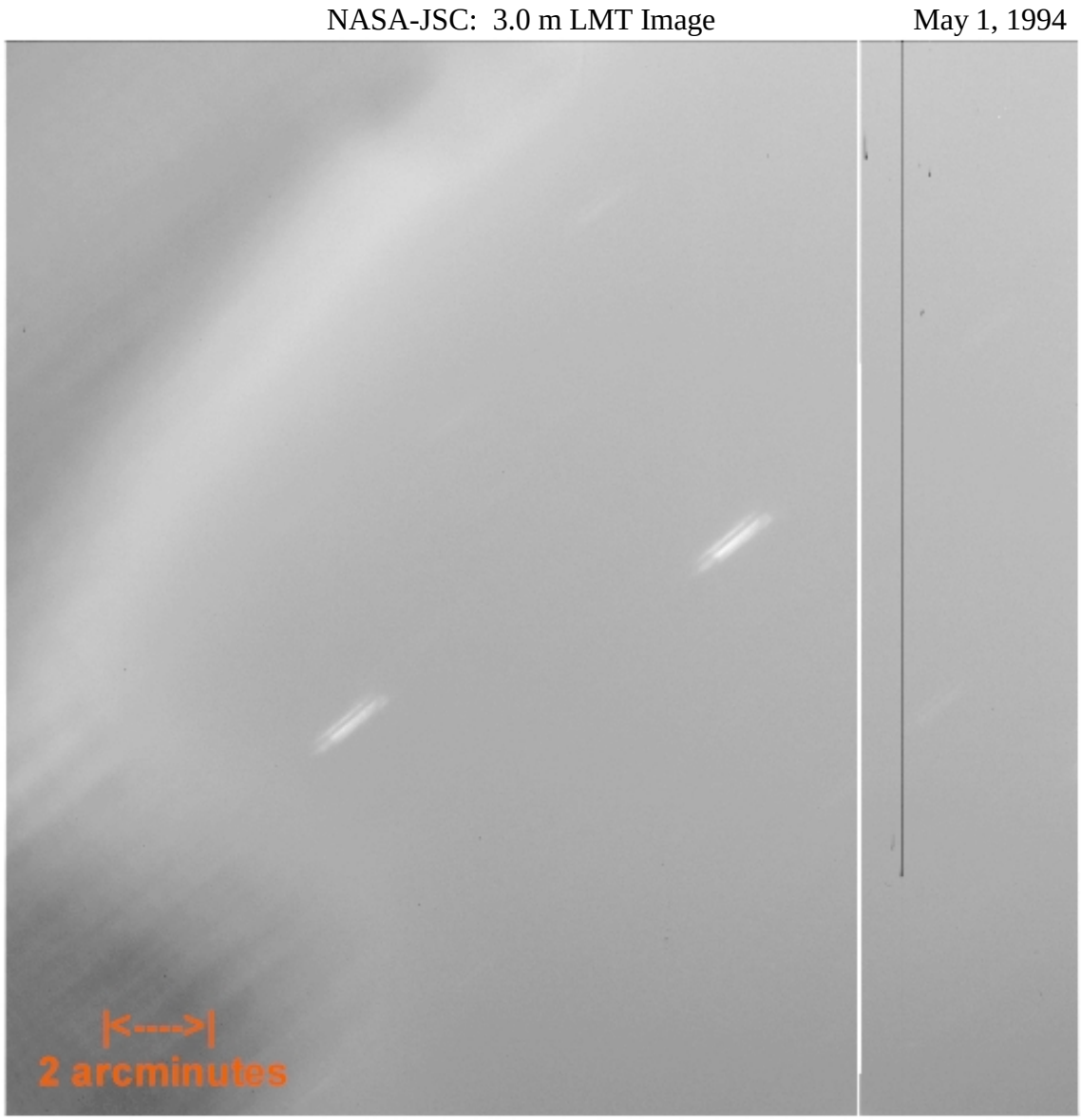

Figure II.B-24. Image acquired with the 3 m NASA-LMT at NASA-JSC during the first evening of observations on May 1st, 1994. The image shows several stars gradually coming into focus in this 2x2 binned white-light image of approximately 90 second exposure time. The field shows obscuration due to the formation of condensation on the camera head CCD window. The CCD is rotationally misaligned and the read rate does not match the sidereal drift hence the angled and trailed star images.

NASA-JSC: 3.0 m LMT Image May 1, 1994

Figure II.B-25. Image acquired with the 3 m NASA-LMT at NASA-JSC during the first evening of observations on May 1st, 1994. The image shows several stars gradually coming into focus and proper orientation for sidereal drift scanning in this 2x2 binned white-light image of approximately 90 second exposure time. The condensation on the camera head CCD window has cleared somewhat due to the brief application of dry nitrogen. The CCD is approximately rotationally aligned, but the read rate does not match the sidereal drift hence the trailed star images.

NASA-JSC: 3.0 m LMT Image June 1994

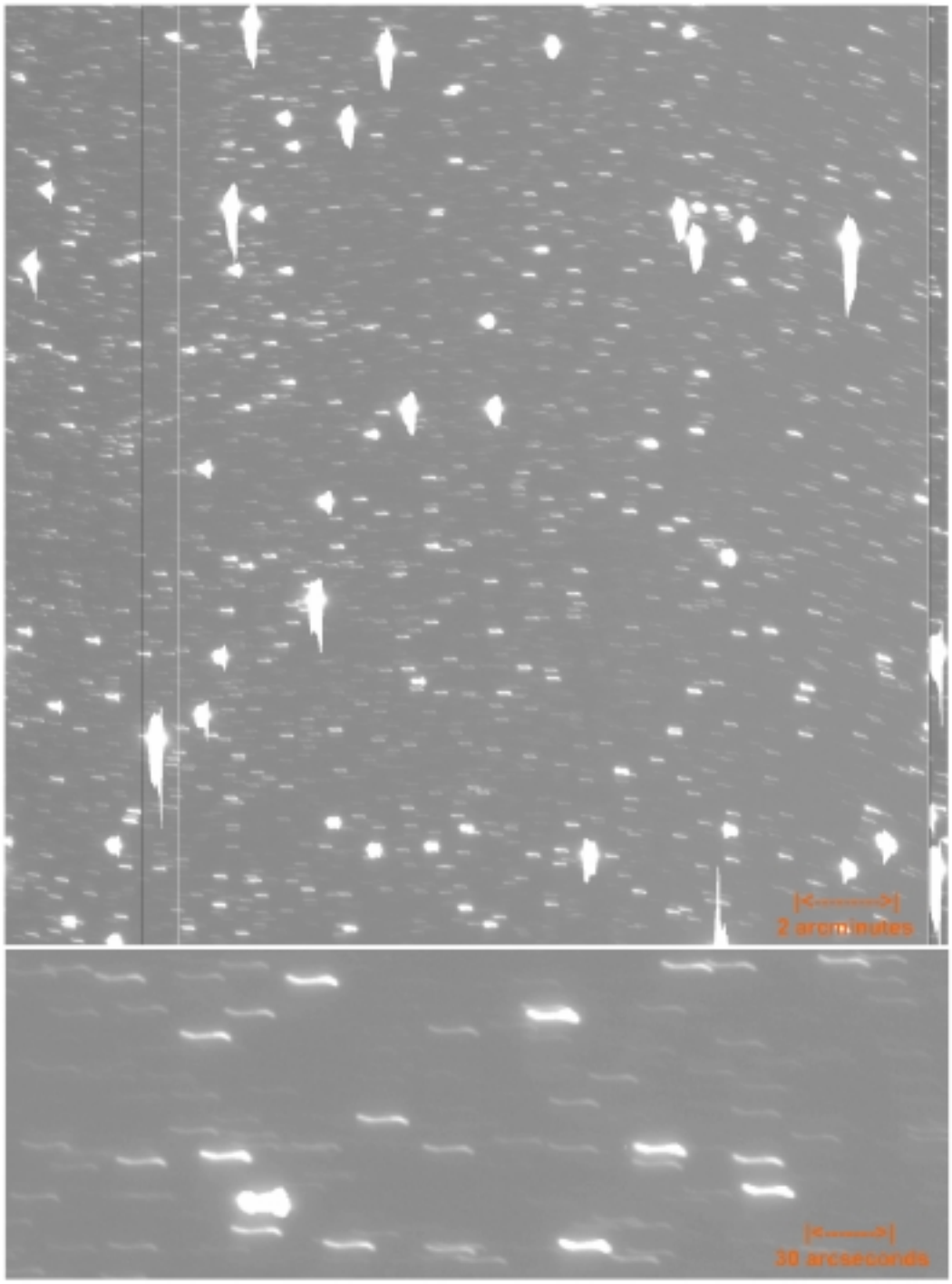

Figure II.B-26. Image acquired with the 3 m NASA-LMT at NASA-JSC during alignment trials in June, 1994. The image shows an approximately accurate read rate, but improper CCD rotational orientation in this un-binned white-light image of approximately 96 second exposure time. The S-shaped nature of the stellar trails is due to the corrector residual field distortion causing a variable velocity of stellar motion as they transit the FOV.

NASA-JSC: 3.0 m LMT Image June 1994

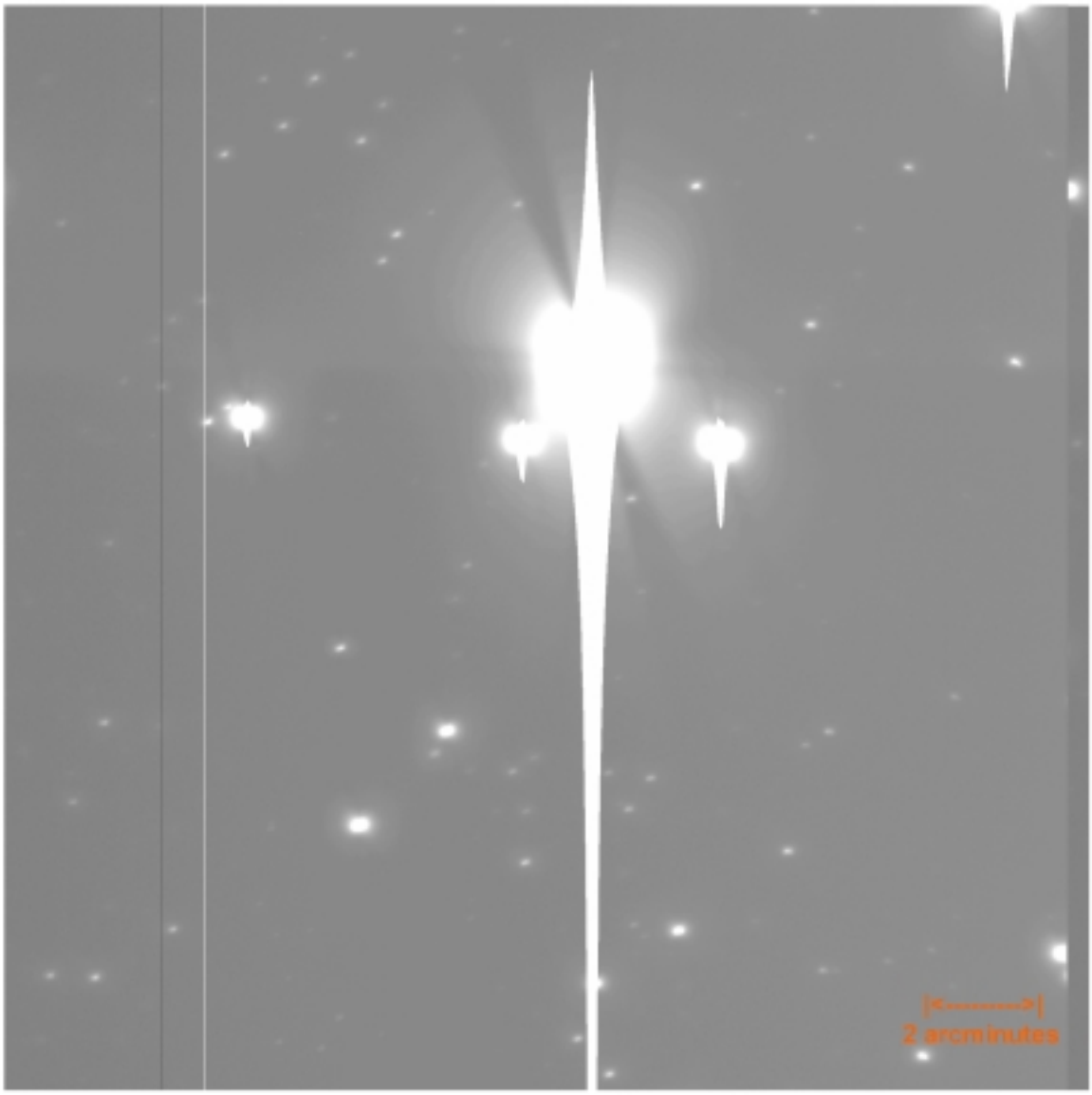

Figure II.B-27. Image acquired with the 3 m NASA-LMT at NASA-JSC during alignment trials in June, 1994 approximately one month after first light. The image shows relatively good CCD read rate and CCD rotational alignment with the sidereal drift rate and direction. There is still some orthogonal drift however. This un-binned white-light image has an approximately 96 second exposure time.

NASA-JSC: 3.0 m LMT Image July 1994

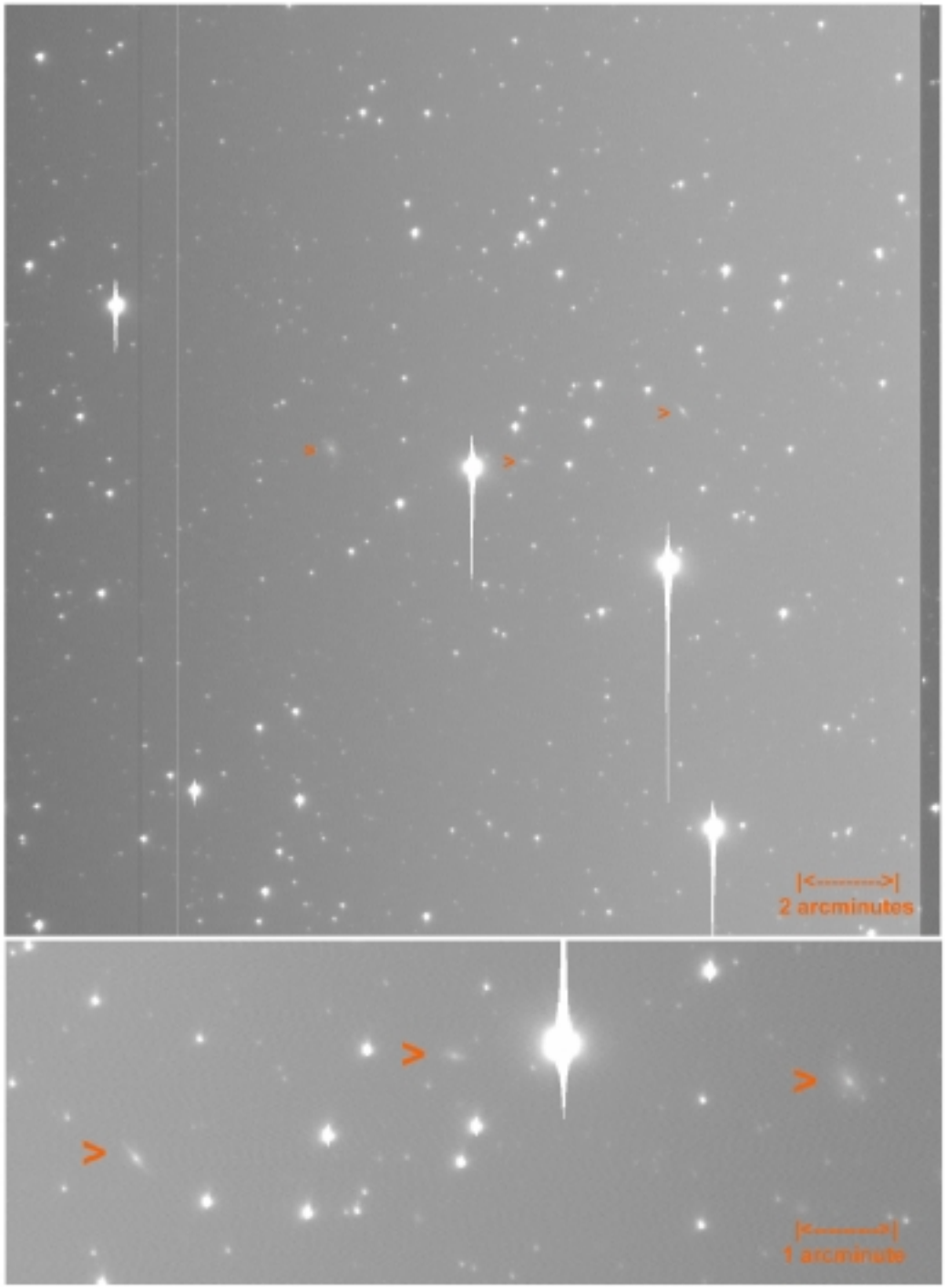

Figure IIB-28. Image acquired with the 3 m NASA-LMT at NASA-JSC after the completion of alignment trials in July, 1994, approximately two months after first light. The image shows a star field at a moderate resolution of 2.8 arcseconds. The field contains the first galaxies (three red arrows) observed by the NASA-LMT. This is a white-light sidereal drift-scanned image with 96 second exposure time.

NASA-LMT @ JSC: 2.5 arcsec FWHM Image August 1994

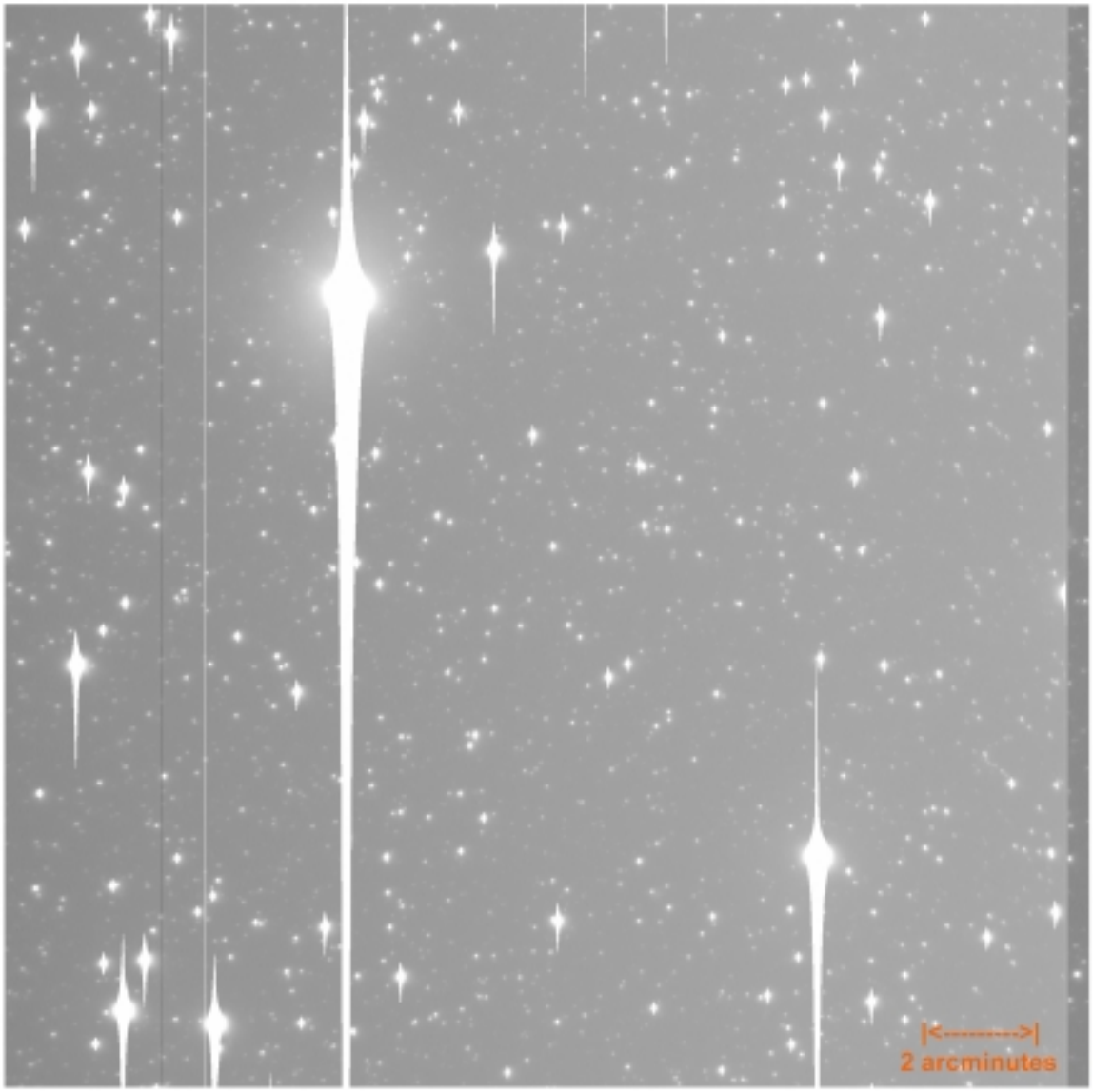

Figure II.B-29. Image acquired with the 3 m NASA-LMT at NASA-JSC after the completion of alignment trials in August, 1994, approximately three months after first light. The image shows a star field at a moderate resolution of 2.5 arcseconds FWHM. The image is the best achieved by the NASA-LMT at the NASA-JSC location. It was of sufficient quality to prompt a search for a more suitable dark-sky location for the NASA-LMT. This is a white-light sidereal drift-scanned image with 96 second exposure time.

critical since the mercury vapor hazard was significant under Houston's high ambient temperature conditions (Chapter IV).

C. NASA-LMT – NODO Development

The importance of having an observing site with minimal sky brightness was demonstrated in Figures II.B-1 through 5. Moving from the NASA-JSC site with a sky brightness of 16.0 mag/arcsecond^2 to a high altitude mountain site away from urban areas with a 22.0 mag/arcsecond^2 sky brightness would yield an approximate 2.5 magnitude gain in sensitivity for both DM detection of orbital objects and sidereal detection of astronomical objects. A darker sky coupled with the improved atmospheric seeing at high altitude, as opposed to the sea level JSC site, would enable the NASA-LMT to perform optimally. As discussed later in Chapter IV, the high ambient temperatures in Houston also exacerbated the Hg vapor hazard by increasing the evaporation rate and extending the time for the mirror to fully oxidize. Whereas at NODO the Hg vapor concentration after mirror formation normally drops within a day or two to levels which allow work without a respirator, at JSC this was rarely the case even a week after mirror formation. Thus a cooler high-altitude site was desirable from a safety perspective.

The NODO facility was found serendipitously during a June 1994, observing campaign to the National Solar Observatory (NSO), located in Sunspot, NM. The author had accompanied Drew Potter in support of his observations of the lunar exosphere using

the 40 cm Evans Coronagraph. During the visit we inquired as to the existence of any surplus facilities which we might use to house the newly operational NASA-LMT. Several employees directed us to what was known at the time as the Cloudcroft 48-inch Facility located in the Lincoln National Forest 3 km north of Cloudcroft, NM or about 29 km north of Sunspot (Figure II.C-1). The facility had been constructed by the US Air Force (USAF) in 1965 and had once housed a 48-inch diameter (1.22 m) Cassegrainian telescope that, ironically, was used to track both orbital satellites and missiles launched from White Sands Missile Range located in the desert below. Accompanied by NSO facilities director Rex Hunter, we visited the site and found it immediately ideal for housing the NASA-LMT. Besides being a high-altitude site (2774 m) with dark skies (V Band 21.81 mag/arcsecond^2; Schneeberger et al. 1979), having an average of 200 clear nights annually with mean seeing between 1.2 and 1.6 arcseconds (Smith and Salisbury 1961), and cool ambient temperatures (maximum recorded high temperature of 28 ^0C), the observatory structure itself was well suited for an LMT. The 4.25 m wide dome slit was hemispherical and thus was completely un-obscured at zenith. Additionally the monolithic pier was isolated form the building and its upper surface matched the 3.5m square footprint of the LMT as illustrated in Figure II.C-2.

The facility also had all of the infrastructure support required to assemble and yield an operational LMT. Besides having NSO and Apache Point Observatory (which possessed a sophisticated weather monitoring station) nearby, amenities such as a machine shop, an operational 3-ton crane, phone and Internet service, and kitchen/restroom facilities existed at the site. The discovery of the Cloudcroft site

NODO Facility Location 3 km North of Cloudcroft, NM

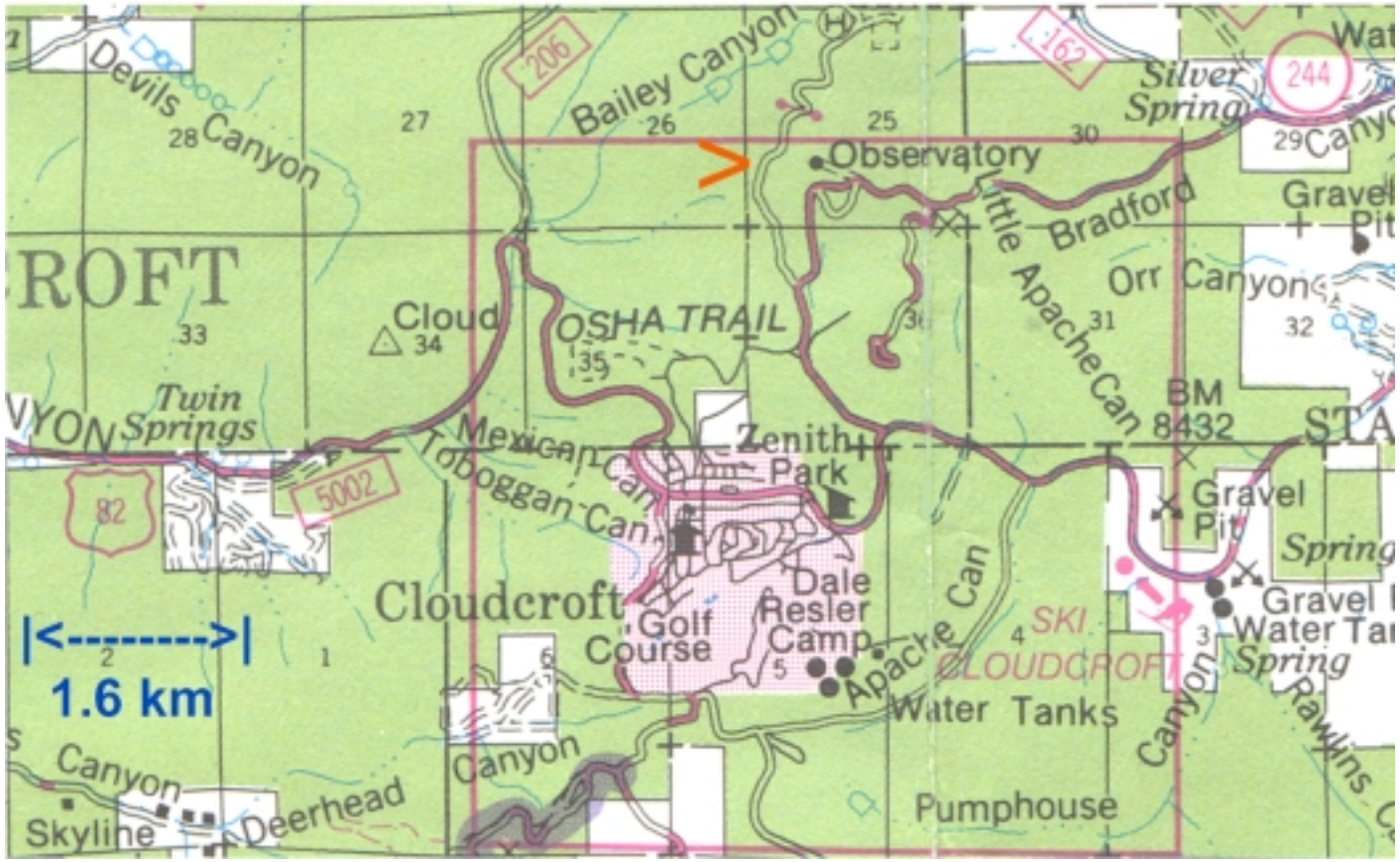

Figure II.C-1. A map showing the location of NODO facility 3 km north of Cloudcroft, NM. The observatory (indicated by the red arrow) sits on a hilltop within the Lincoln National Forest at 2772 m altitude. The site is 170 km northeast of the nearest major airport in El Paso, TX. The proximity of Cloudcroft does not pose a serious light pollution problem due to lighting controls and its small population (800).

NODO Facility and NASA-LMT Cross-sectional View

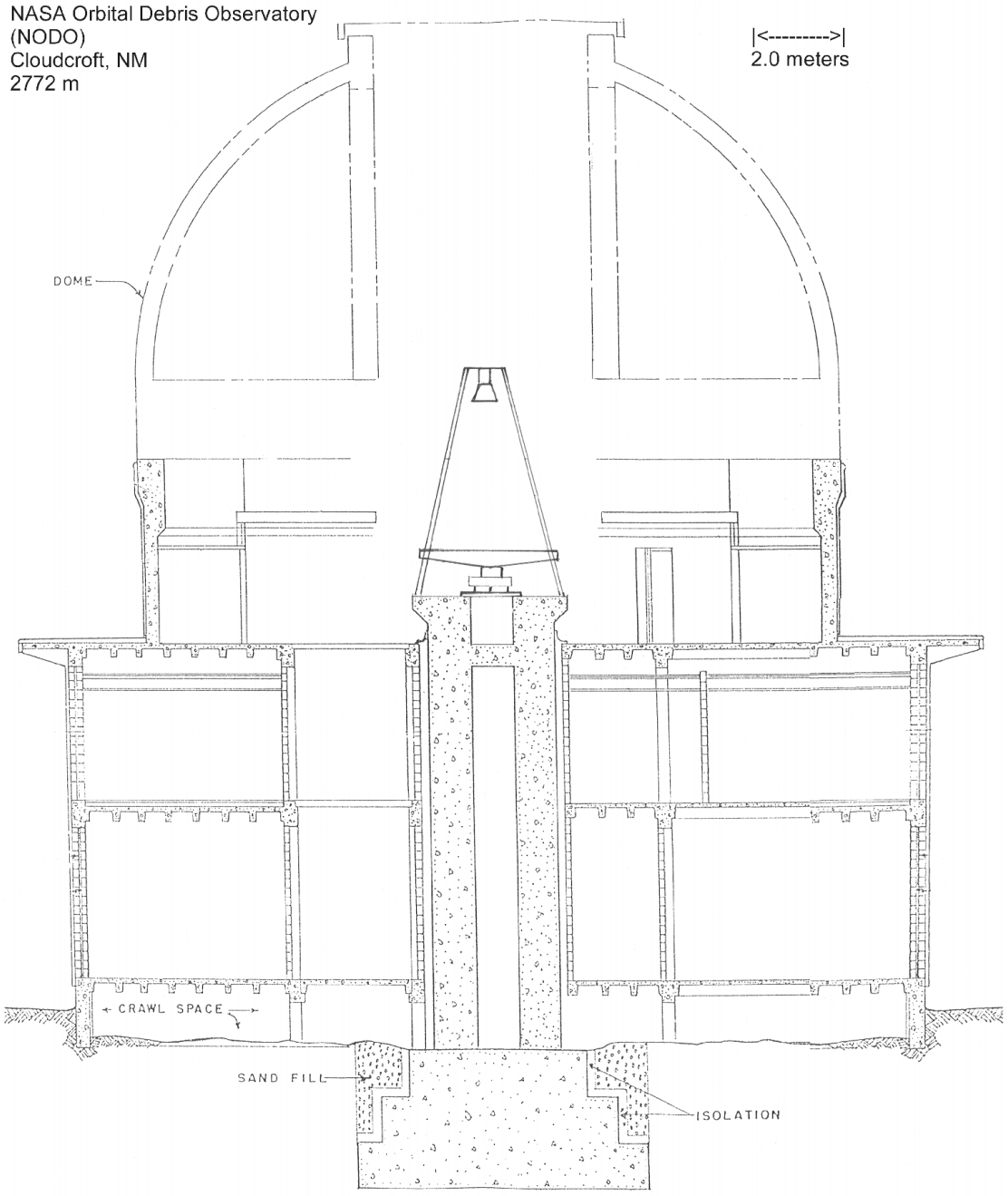

Figure II.C-2. Interior cross-sectional view of the NASA Orbital Debris Observatory (NODO) and the 3.0 m NASA-LMT located within. The LMT footprint matches the 3.35 m square upper surface of the central concrete pier which originally held a 1.2 m diameter conventionally mounted Cassegrain telescope. The pier is physically isolated from the building and extends 3.3 m into the bedrock beneath the facility. The building, pier, and dome slit could easily accommodate a 6.0 m LMT with straightforward modification of the dome floor. The diagram is to correct scale.

immediately ended the site search and consideration of the leading candidate at the time – the White Sands Test Facility (WSTF) near Las Cruces, NM which was an adjunct to NASA-JSC. Had the NASA-LMT been placed at WSTF it would have likely failed due to extreme temperatures and dusty conditions. NASA was not able to move the LMT into the new facility immediately since it was in a state of disrepair. It had been abandoned 12 years previously (1982) after the completion of a 4 year National Science Foundation (NSF) funded project which had operated the former USAF 1.22 m diameter Cassegrain as a photometric survey instrument (Africano PC). Unfortunately after being abandoned, the roof had leaked severely and much of the interior required cleaning and remodeling. Surprisingly however, most of the mechanical systems including the dome slit mechanism, the crane, and the exhaust ventilation were still operational. Repairs were effected by NSO personnel and paid for by NASA-JSC through an arrangement orchestrated by Rex Hunter and Drew Potter which allowed NASA to lease the facility without charge from NSF as long as NASA covered the maintenance costs. This arrangement was mutually beneficial as it relieved US Forest Service pressure on NSF to demolish the five million dollar facility and return the site to its natural state.

The move from the NASA-JSC silo was performed in January 1995 with the ambitious goal of having the telescope fully operational again by May 1995. Figure II.C-3 shows one stage in the disassembly of the components within the NASA-JSC silo while Figure II.C-4 illustrates aspects of the reassembly of the LMT at the NODO facility. Figure II.C-5 shows clearly the mirror undercarriage after the I-Beam base was upgraded with an improved 3-point suspension system. Although some aspects of the JSC

NASA-JSC: Disassembly of the LMT System

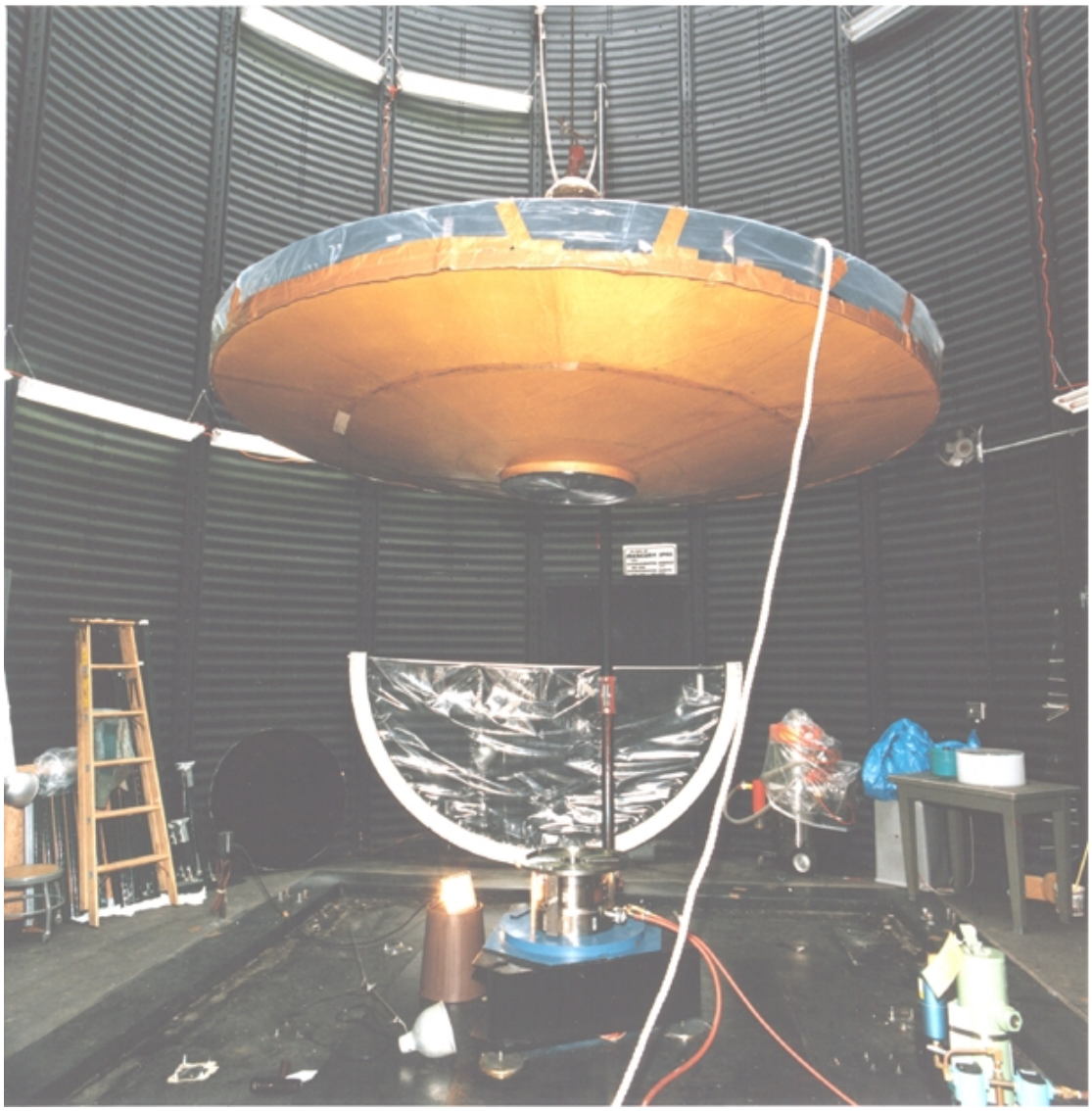

Figure II.C-3. Removal of the NASA-LMT primary mirror from the NASA-JSC Silo in preparation for shipment to NODO. The mirror was removed through the observing aperture in the silo roof. Note the PICo air bearing and I-Beam base at center and the protective Mylar cover and Hg vacuum cleaner at center and right rear respectively. The top of the air system desiccator is visible at right front.

Installation of the LMT at NODO

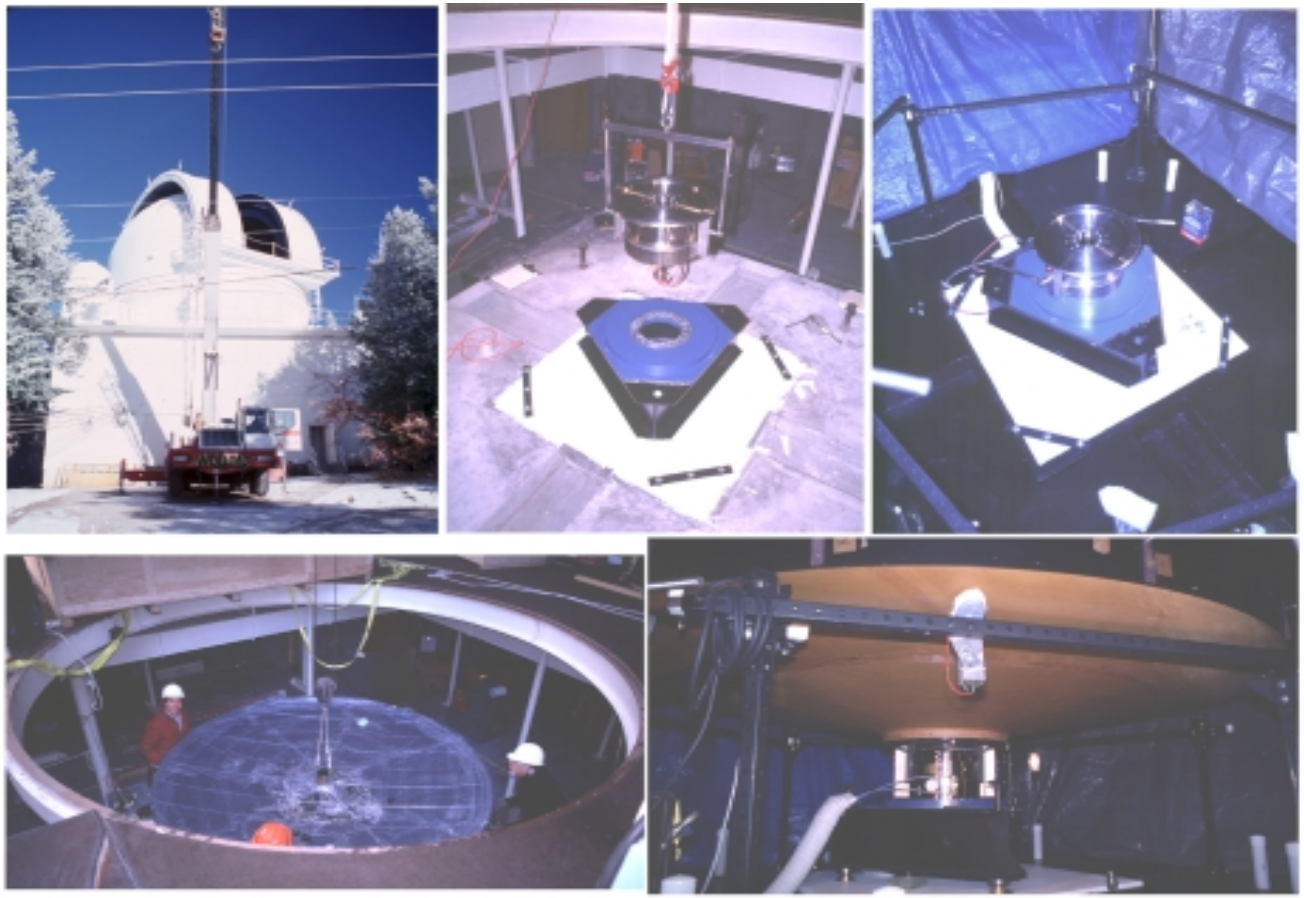

Figure II.C-4. Montage of images recording various stages of the NASA-LMT installation at NODO. Clockwise from left: 1) Insertion via crane of the primary mirror through the dome slit. 2) Lowering the PICo air bearing onto the I-Beam base. 3) Completed mirror safety stabilizer and application of pier sealant. 4) Lowering of the primary mirror on to the air bearing. 5) Completed installation of mirror components (note emergency stop brush in foreground).

NASA-LMT: Primary Mirror Undercarriage

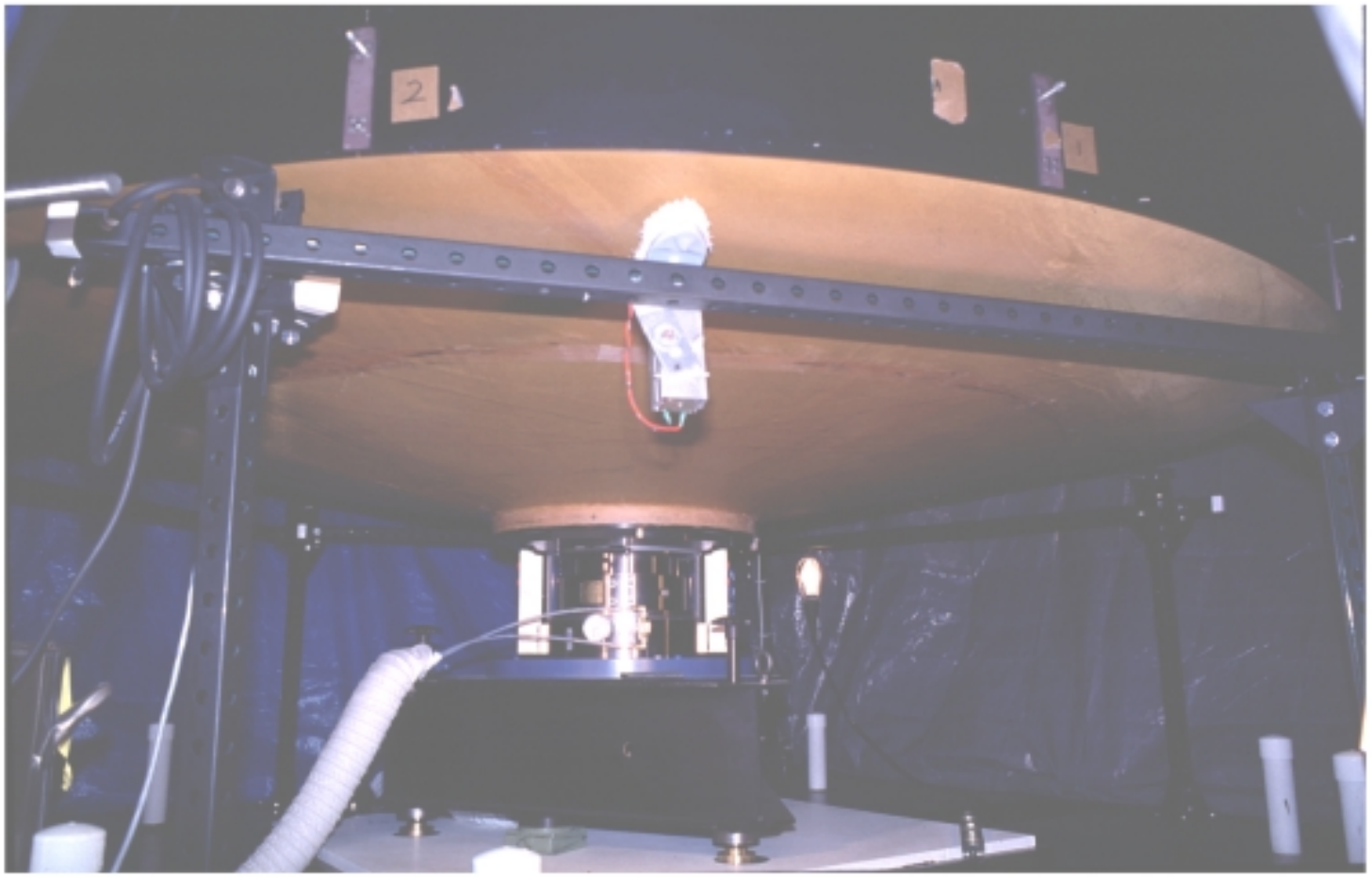

Figure II.C-5. View of the undercarriage of the NASA-LMT primary mirror showing the air bearing, I-beam base, and stabilizer. The brush mounted near the mirror under-surface is part of an emergency braking system which protects the air bearing by stopping the mirror rotation in the event the primary air system depressurizes.

installation were retained, the prime focus assembly and support were completely redesigned for the NODO installation. All parts for the new assembly were fabricated by NASA machinist Bill Davidson and tested at JSC prior to shipment to Cloudcroft to ensure ease of assembly in-situ.

Figures II.C-6 shows a montage of the prime focus array illustrating its modular nature wherein components can be easily accessed and adjusted or removed as necessary. The array incorporates multiple degrees of positioning freedom for both large-scale and precision vertical focus, lateral alignment of the corrector and CCD independently, and tilt alignment of the corrector and CCD independently. The design served well for 5 years but is now being reconfigured for use with the new PV 2K CCD camera which is much larger than the pre-existing cameras. Figures II.C-7 and 8 show the installed PF assembly and the LMT system after a railing was added during the second year of NODO operations. Figure P-1, presented in the Preface, shows the LMT shortly after the initial installation. A recent view of the control room is shown in Figure II.C-9.

The assembly process was straightforward and NODO first light was achieved on April 24th, 1995. Instrument and image quality refinement has continued from that point forward, progressing from the tantalizing but modest images shown in Figures II.C-10 and 11, to the respectable 1.8 arscesond FWHM resolution image in Figure II.C-12, and culminating in exemplary performance like that exhibited second frame of Figure IIC-12. More examples of this type will be shown in Chapter VI. The addition of the new PV 2K CCD in September 2000, with twice the FOV and exposure time, should yield even more spectacular results.

NASA-LMT Prime Focus Array

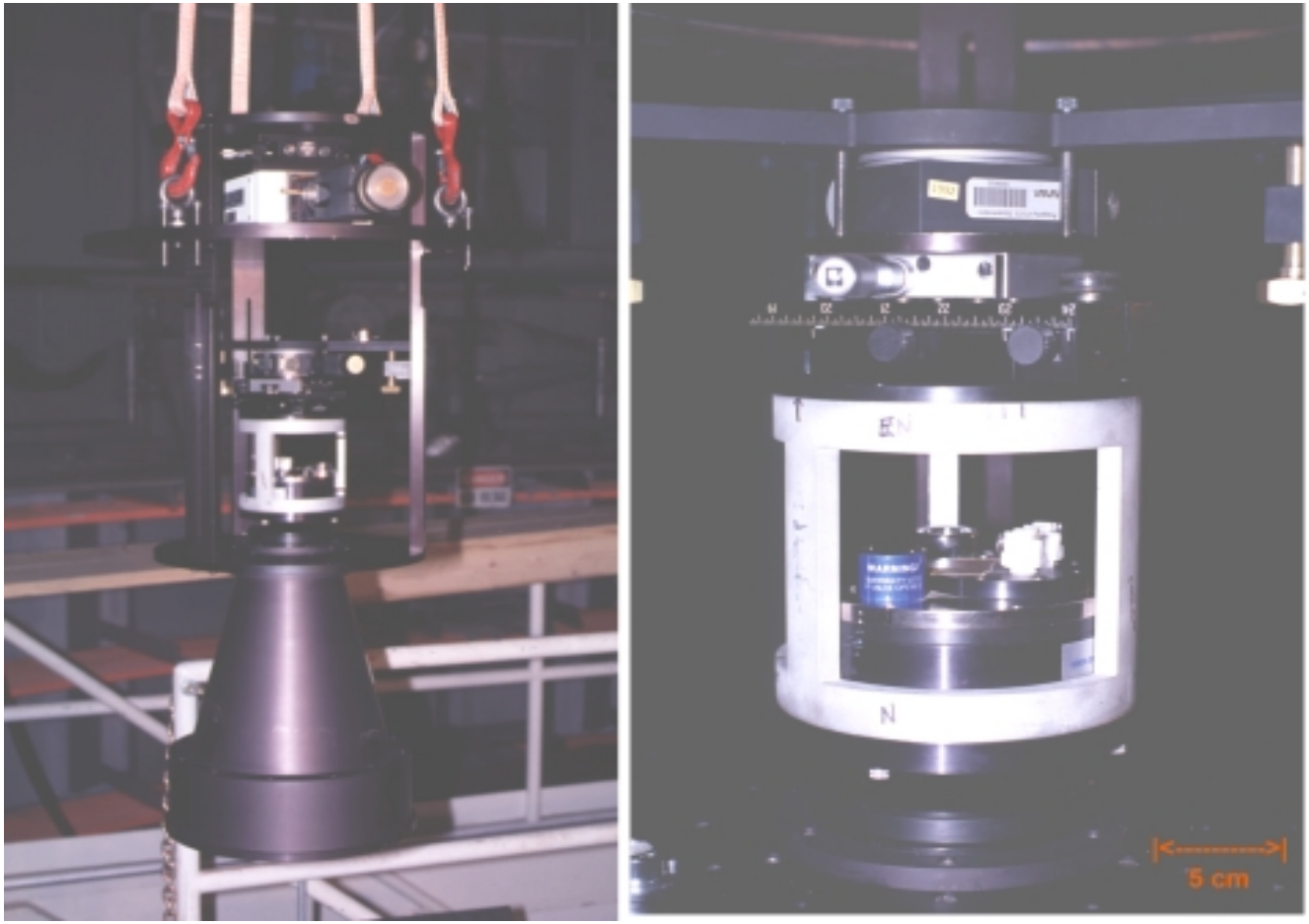

Figure II.C-6. Two views of the prime focus array developed for use at NODO. The modular assembly was designed to be easily removable form the prime focus support structure to facilitate upgrades. Multiple degrees of freedom are enabled for accurate alignment of the CCD (left close-up) and the corrector lens relative to both each other and the primary mirror.

NASA-LMT: Prime Focus Array

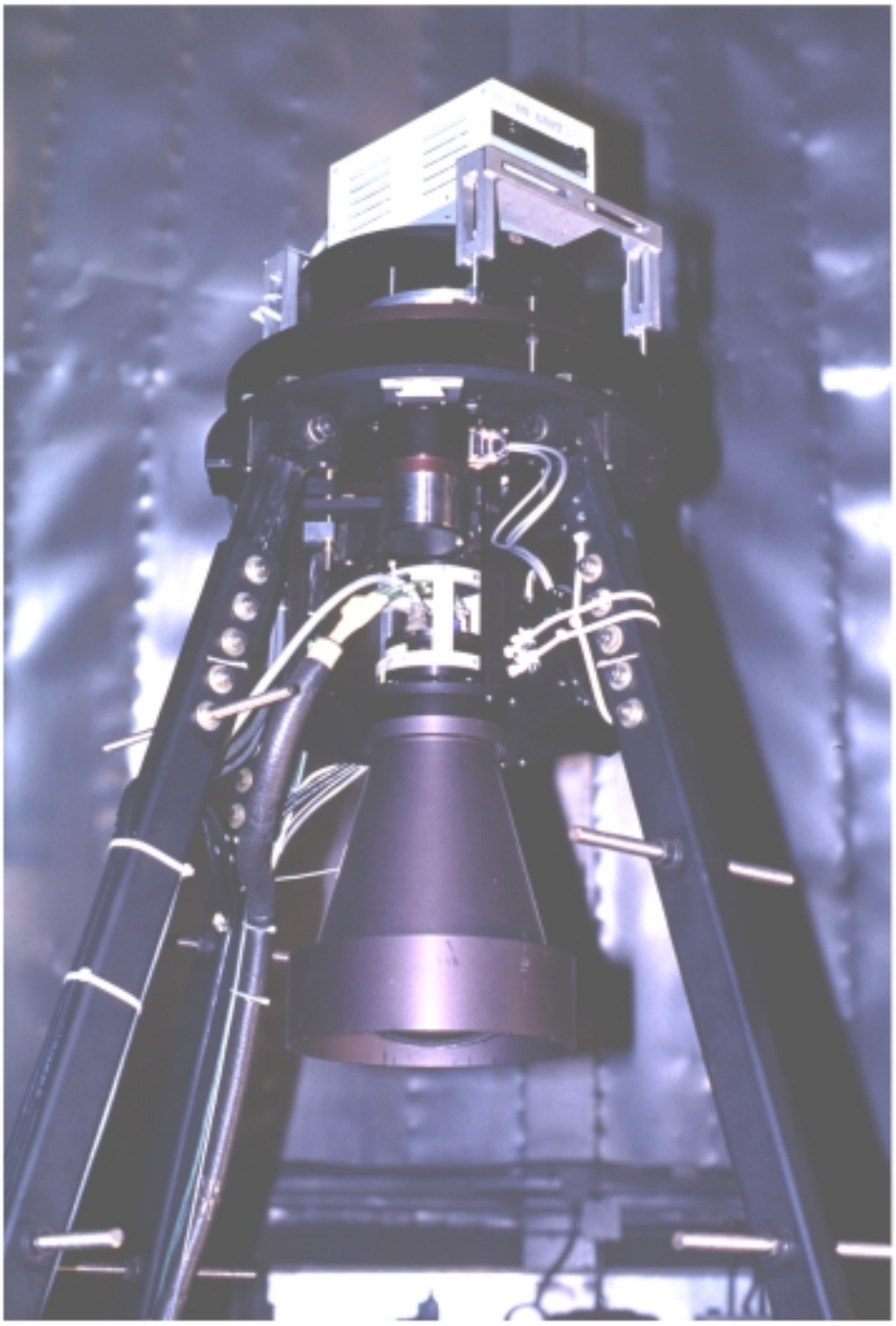

Figure II.C-7. View of the prime focus assembly installed above the NASA-LMT primary mirror. The LSP 2K CCD is installed at the focal position. The first generation orbital object camera is seen installed at its holding station (above center) while not in use. The white box atop the array houses the control electronics for the CCD.

NASA-LMT @ NODO: Liquid Mirror and Prime Focus Array

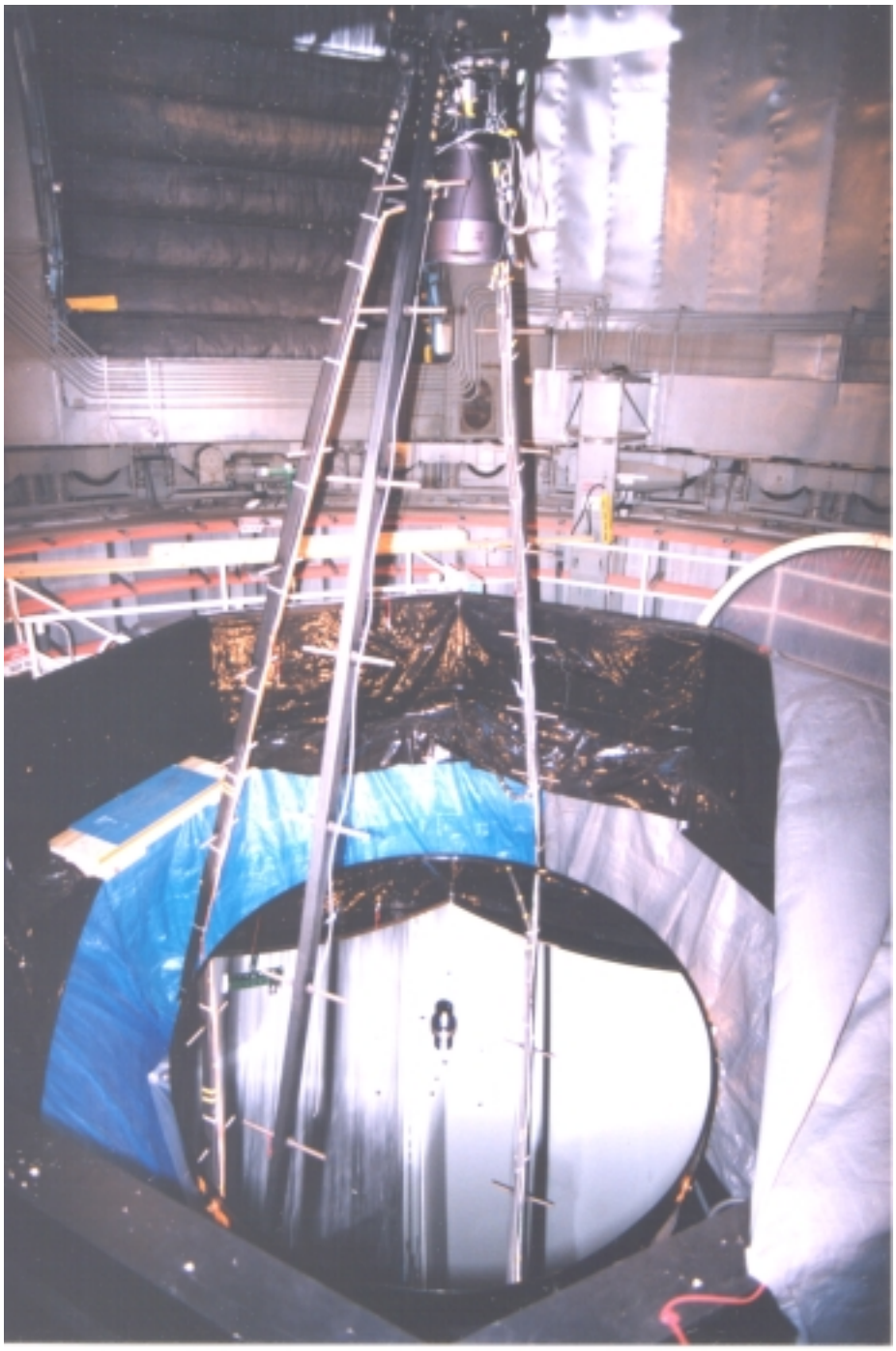

Figure II.C-8. Wide-angle view of the NASA-LMT liquid mirror and the prime focus array installed at NODO. Access to prime focus is achieved by ascending the PF support legs starting from the platform at the left. The protective railing was installed in June 1996.

NODO Control Room

Figure II.C-9. The control room at NODO. The majority of LMT operations are controlled from this room located on the second floor of the NODO facility. Telescope control lines run 40 m from the dome level two stories above. Only the motor controller and the Digital Video (DV) recorder for the orbital object camera are located near the telescope since they require short cable lengths. All equipment is tied to Uninterruptable Power Supplies (UPSs) and an Emergency Generator. Unix machines (left) control the CCD camera, WinTel PCs (right) provide data logging and storage, the Intensified Video camera for orbital object data acquisition is controlled form the station at the rear. All machines are networked with Internet access.

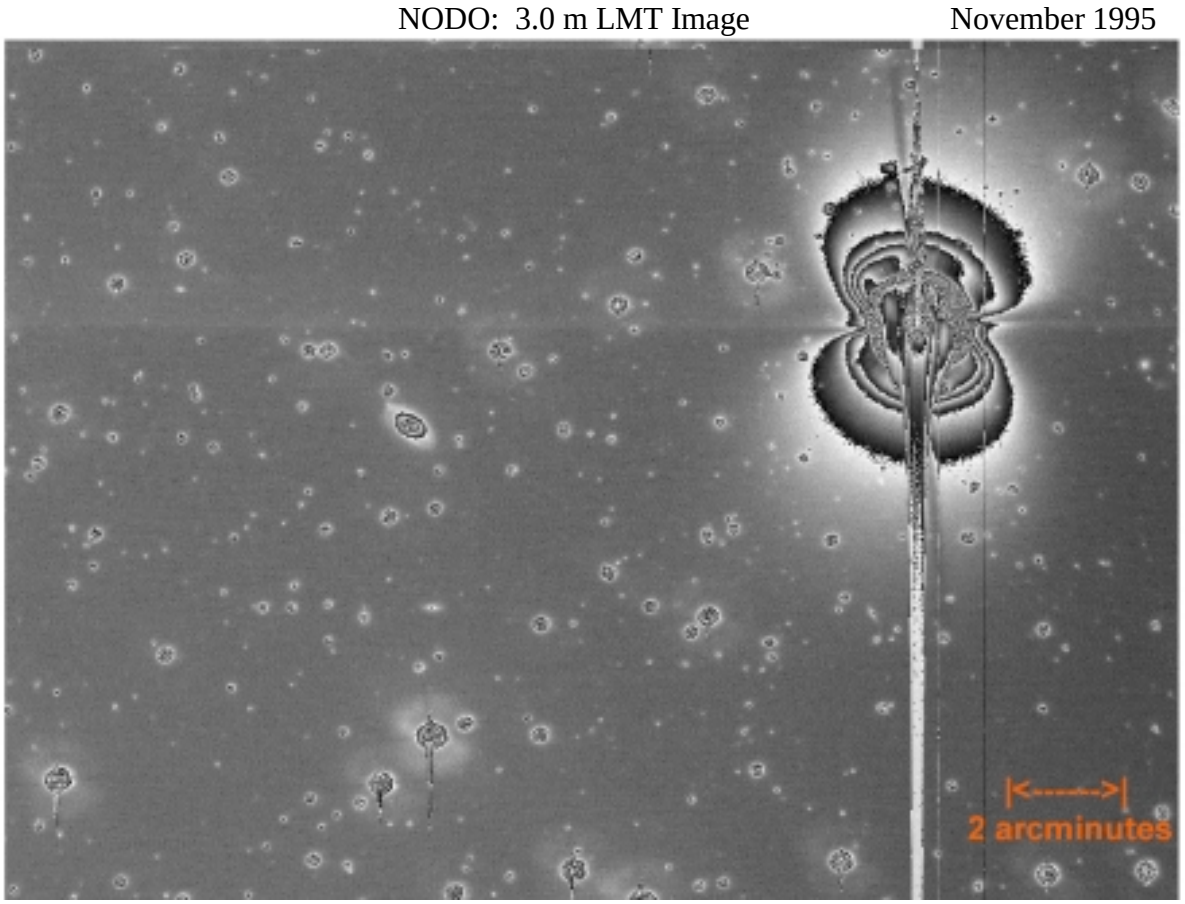

Figure II.C-10. Image acquired with the 3 m NASA-LMT at NODO during alignment trials in the Fall 1995. The image shows a star field at a moderate resolution of approximately 2.0 arcseconds FWHM, but with an S-shaped scattered light pattern. The pattern was eventually eliminated by accurate optical alignment of the mirror and corrector. Many faint galaxies are visible in this image. The display scale uses linear contours to reveal fainter image structure. This is a white-light sidereal drift-scanned image with 97.1 second exposure time acquired with the LSP 2K CCD.

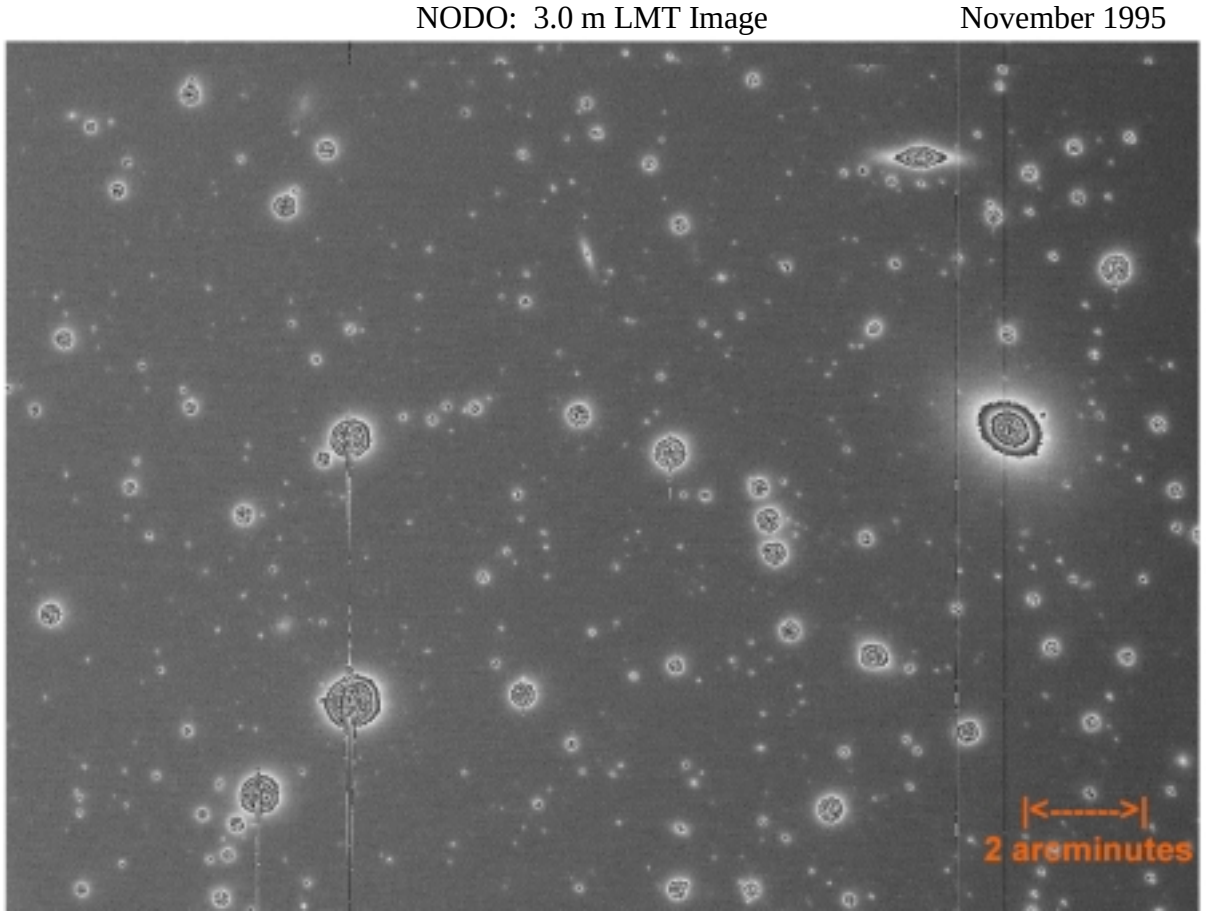

Figure II.C-11. Image acquired with the 3 m NASA-LMT at NODO during alignment trials in the Fall 1995. The image shows a star field at a moderate resolution of approximately 2.0 arcseconds FWHM and the S-shaped scattered light pattern has been eliminated. Many faint galaxies are visible in this image. The display scale uses linear contours to reveal fainter image structure. This is a white-light sidereal drift-scanned image with 97.1 second exposure time acquired with the LSP 2K CCD.

NASA-LMT @ NODO: 3.0 m LMT Image December 1995

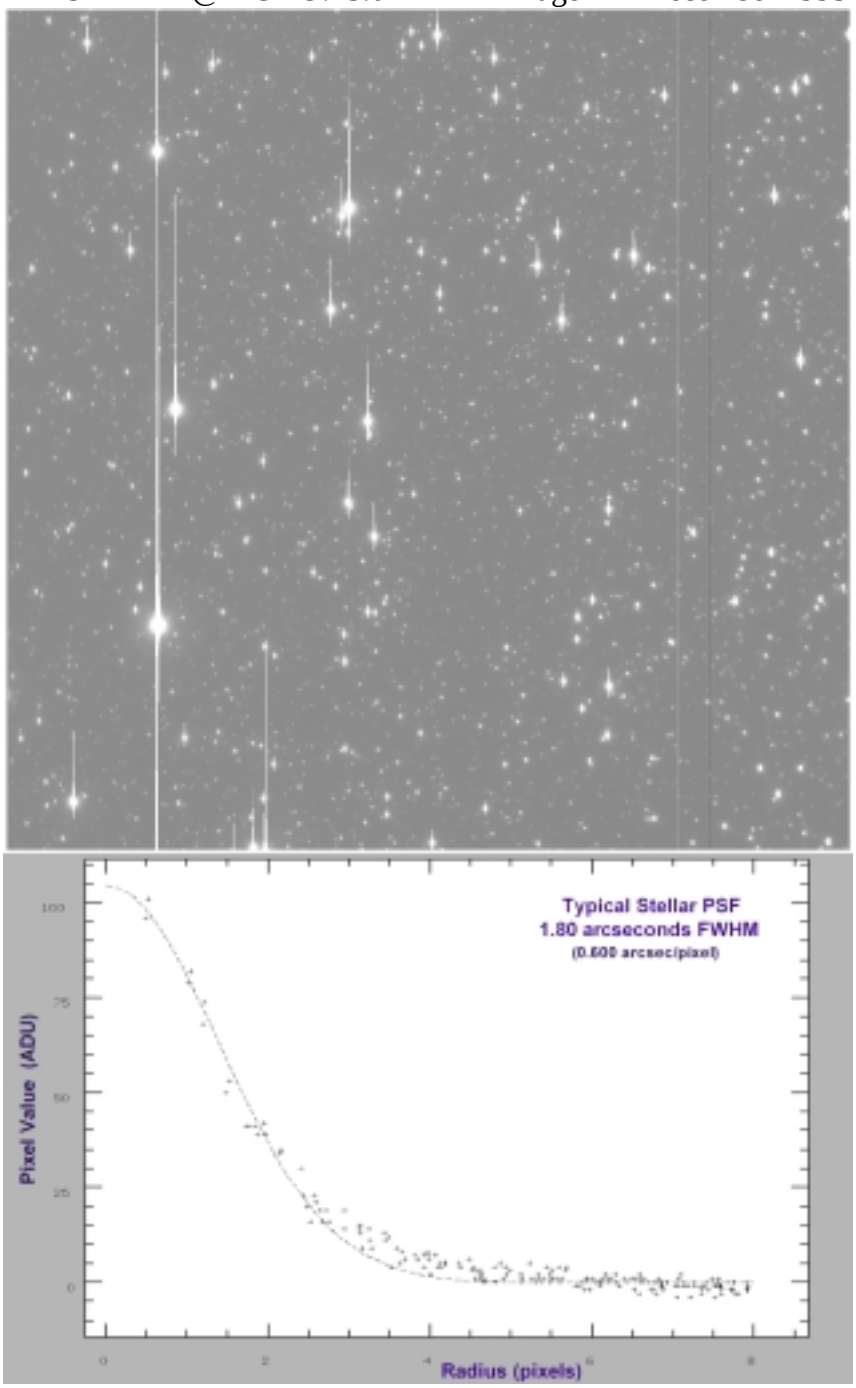

Figure II.C-12. Image acquired with the 3 m NASA-LMT at NODO at the completion of the first phase of alignment trials in December, 1995.The stellar PSFs near the center of this 20.41 arcminute wide field are fit by a Gaussian profile with a 1.80 arcsecond FWHM. Resolution peaked at approximately 1.5 arc-second FWHM in 1997. Afterwards, removal of the field distortion by modifying the corrector lens enabled resolution of 1.0 arcsecond FWHM to be obtained on rare occasions of exceptional seeing. This is a white-light sidereal drift-scanned image with a 97.1 second exposure time. N left, W up.

NASA-LMT @ NODO: Image Quality Progression

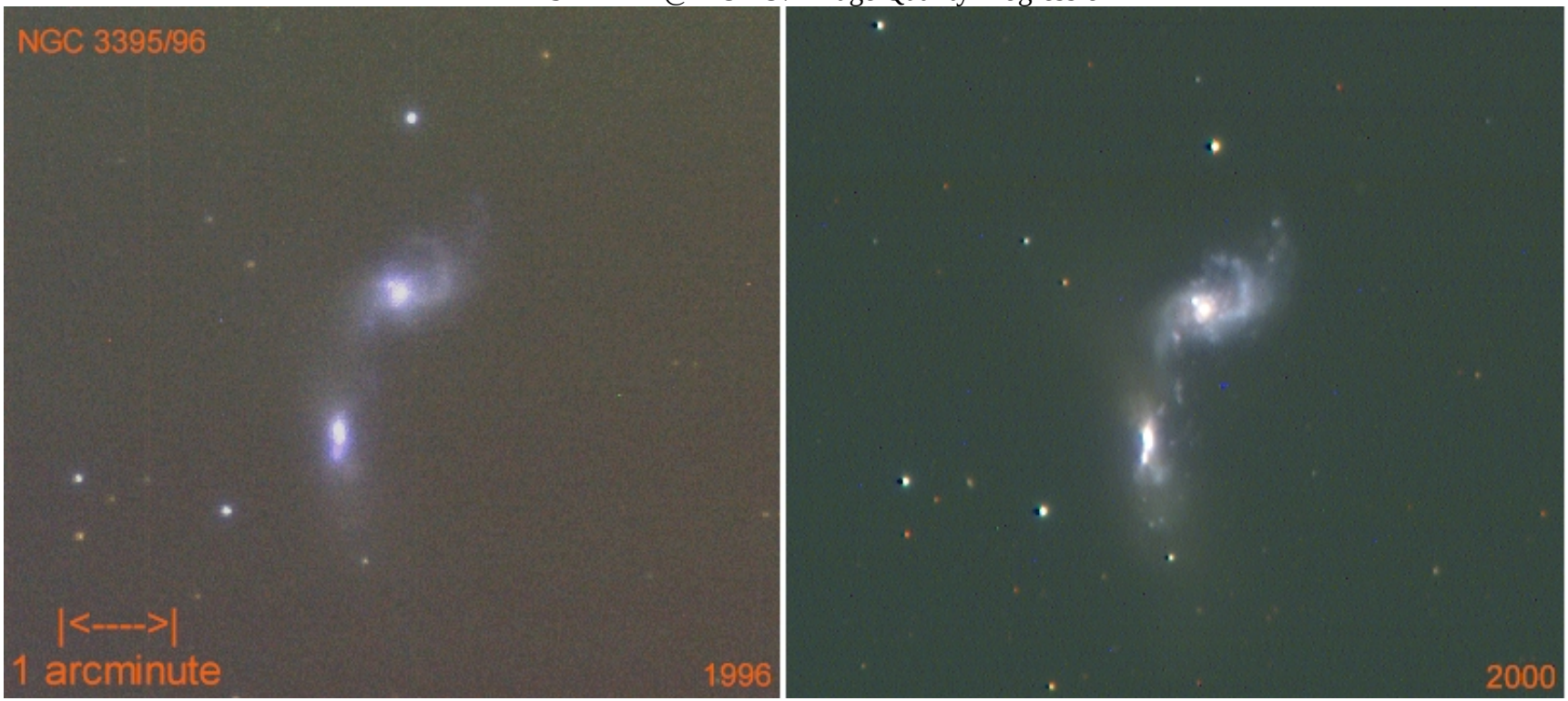

Figure II.C-13. A comparison of images of the interacting galaxy pair NGC 3395/3396 demonstrating image quality improvements due to instrument refinement. The image on the left is a 3-color composite generated from data acquired through three different filters (BVR) on three different nights during the Spring 1996 and 1997 observing seasons with the LSP 2K CCD. The image on the right was similarly generated from observations made during the Spring 1999 and 2000 observing season with the PV 1K CCD. Despite the fact that the PV 1K has reduced resolution and exposure time (0.960 arcsec/pix and 78.1 sec versus 0.598 arcsec/pix and 97.1 sec for LSP 2K), the latter image is of significantly higher quality due to instrument refinements. These refinements include a thinner Hg layer, an improved motor controller, a more quantum efficient CCD, a modified optical corrector and importantly - accurate dynamic balancing of the primary mirror and alignment of the prime focus array. N left ,W up.